

1 **MS 8001 Revision 1**

2 **MSA Presidential Address**

3 **Petrogenetic and Tectonic Interpretation of Strongly Peraluminous Granitic Rocks and**
4 **their Significance in the Archean Rock Record**

5 Carol D. Frost^{1*} and Fabio A. Da Prat^{1*#}

6 ¹Department of Geology and Geophysics, University of Wyoming, Laramie WY 82071

7 *frost@uwyo.edu and fadaprat@gmail.com

8 [#]Present address: Rio Tinto Kennecott, 4700 W Daybreak Pkwy, South Jordan, UT 84009

9 **Abstract**

10 Strongly peraluminous granitic rocks (SPG), defined by an aluminum saturation index
11 greater than 1.1, become abundant in the rock record in the Neoproterozoic. This study identifies
12 three different varieties of Neoproterozoic SPG in the Archean Wyoming Province, USA. These
13 include calcic SPG, represented by the Webb Canyon Gneiss and Bitch Creek Gneiss of the
14 Teton Range; calc-alkalic to alkali calcic suites composed entirely of SPG, including the Rocky
15 Ridge garnet granite gneiss of the northern Laramie Mountains and the Bear Mountain granite in
16 the Black Hills; and calc-alkalic to alkali-calcic suites that include both weakly and strongly
17 peraluminous granitic rocks, such as the Mount Owen batholith, Wyoming batholith, and Bears
18 Ears intrusion. Although the petrogenesis of all the SPG suites involves partial melting of crustal
19 sources, the composition of those sources, the melting conditions, and the tectonic settings vary.
20 The calcic suites originate by dehydration melting or water excess melting of hornblende-
21 plagioclase rocks at relatively high temperature. The suites composed entirely of SPG form by
22 partial melting of metasedimentary rocks by reactions involving muscovite at lower
23 temperatures. Suites with both weakly and strongly peraluminous granite may form by partial

24 melting of metasedimentary rocks by reactions involving biotite, or by assimilation of aluminous
25 melts of felsic crust by differentiated calc-alkalic magma. Most of the Wyoming SPG appear to
26 have formed in collisional orogens, but SPG of the Wyoming batholith and Bears Ears granite
27 are associated with continental arc magmatism. The appearance of SPG in the Neoproterozoic rock
28 record marks the time when subduction enabled the formation of strong, thick, increasingly felsic
29 continental crust, which in turn allowed development of a mature, clastic sedimentary cover.
30 Lateral movement of crustal blocks led to collisional orogeny, SPG magma genesis, and the
31 formation of the first supercontinents.

32 **Introduction**

33 Peraluminous rocks contain more Al than can be accommodated in feldspars alone
34 (Shand, 1947). Shand defined the aluminum saturation index (ASI) as the molecular ratio
35 $\text{Al}_2\text{O}_3/(\text{CaO} + \text{Na}_2\text{O} + \text{K}_2\text{O})$. ASI will be 1.0 for any combination of plagioclase and alkali
36 feldspars because alkali feldspars have 1 mole of Al and 1 mole of Na and/or K
37 and anorthite has 2 moles of Al for 1 mole of Ca. The calculation of ASI commonly includes a
38 correction for the presence of calcium in apatite, assuming all phosphorus in the rock is in
39 apatite. The expression for ASI, including this correction, is:

40

$$41 \text{ ASI} = (\text{wt. \% Al}_2\text{O}_3/101.94) / (\text{wt. \% CaO}/56.08 - 3.33 * \text{wt. \% P}_2\text{O}_5/141.95 + \text{wt. \%} \\ 42 \text{ Na}_2\text{O}/61.982 + \text{wt. \% K}_2\text{O}/94.2)^1$$

43 where the denominators are molecular weights of the respective oxides.

¹ Note that the coefficient for the phosphorus correction was incorrectly reported as 1.67 rather than 3.33 in Frost et al. (2001) and Frost and Frost (2008).

44 The aluminum saturation index differentiates peraluminous rocks, with $ASI > 1.0$, from
45 metaluminous rocks, with $ASI < 1.0$. Peraluminous rocks may be further subdivided into weakly
46 peraluminous ($1 < ASI < 1.1$) and strongly peraluminous varieties ($ASI \geq 1.1$) (Bucholz and
47 Spencer, 2019; Sylvester, 1998).

48 Because peraluminous rocks have more molecular Al_2O_3 than can be accommodated in
49 feldspars alone, one or more other aluminous phases must be present. For weakly peraluminous
50 rocks, this phase may be aluminous biotite, but for strongly peraluminous rocks the phases can
51 include muscovite, cordierite, garnet, tourmaline, topaz, spinel, corundum or an Al_2SiO_5
52 polymorph. The aluminous phases may be of magmatic origin, or may be entrained peritectic,
53 restitic, or inherited crystals.

54 Strongly peraluminous granitic rocks (SPG) are commonly interpreted to derive from
55 sedimentary sources (Chappell and White, 2001). Fine-grained clastic sedimentary rocks are
56 aluminous as a result of removal of elements including Na and Ca during weathering and the
57 formation of clays. Metamorphism and partial melting of such aluminous sources produce
58 granite with peraluminous compositions (Nabelek, 2020). Strongly peraluminous granitic rocks
59 formed by partial melting of metasedimentary rocks are potential monitors of source rock
60 composition and temperature of partial melting (Bucholz and Spencer, 2019; Sylvester, 1998).
61 However, to identify the source characteristics of strongly peraluminous granitic rocks, it is also
62 necessary to take into account the specific melting reactions involved and the effect of
63 subsequent magmatic processes, including flow segregation, assimilation, fractionation, and
64 hydrothermal alteration (Clarke, 2019). Mayne et al. (2020) developed models to accommodate
65 the changing bulk source composition during progressive melting and sequential segregation of
66 partial melts from metapelitic rocks to reconstruct more accurately the composition of the source.

67 Although most studies focus on SPG that are derived from metasedimentary crust,
68 especially metapelitic rocks, other sources and mechanisms for the production of SPG are also
69 possible including anatexis of mafic rocks, partial melting of quartzofeldspathic rocks,
70 fractionation of low ASI minerals from a differentiating magma, and vapor phase removal of
71 alkalis (Miller, 1985). Clarke (2019) identified additional processes for the formation of SPG,
72 including diatexis of a metasedimentary rock followed by partial to complete removal of the
73 restite, and contamination of a less aluminous magma by peraluminous metasedimentary rocks.

74 Well-studied Phanerozoic SPG intrusions occur primarily within collisional orogens
75 (Nabelek, 2020; Sylvester, 1998). Emplacement of SPG typically post-dates metamorphism
76 (Nabelek, 2020). In other tectonic environments, including continental arcs and extensional
77 environments, small proportions of granite with $ASI \geq 1.1$ may be present as components of
78 intrusions with a range of silica and ASI (e.g., Brown et al., 2018; Stoesser and Frost, 2006).

79 Strongly peraluminous granitic rocks first become abundant in the Neoproterozoic (Bucholz
80 and Spencer, 2019; Laurent et al., 2014). Neoproterozoic rocks of the Wyoming Province include a
81 number of intrusive suites composed either entirely of SPG or that contain a prominent SPG
82 component. The purpose of this paper is to examine these Neoproterozoic SPG occurrences to
83 establish the characteristics of Archean SPG within a single craton, and to determine the sources
84 and processes that formed them. This information helps to establish whether the full range of
85 modern SPG-forming processes were operating as early as the Neoproterozoic, and has implications
86 for the evolution of Earth's tectonic processes.

87

88 **Neoproterozoic SPG of the Wyoming Province**

89 The Wyoming Province is a block of Archean crust with origins that extend back to the
90 Hadean (Frost et al., 2017; Mueller and Wooden, 2012). Neoproterozoic SPG occur across the
91 Wyoming Province, from the Teton Range in the west to the Black Hills in the east (Fig. 1). This
92 paper focuses on six Neoproterozoic intrusive granitic suites with significant proportions of SPG
93 that have been sufficiently well-studied that the geologic context, and petrologic and
94 geochemical character can be reasonably well-described. Three of the SPG-bearing suites are
95 exposed in the Teton Range: the 2.68 Ga Webb Canyon gneiss, the 2.68 Ga Bitch Creek gneiss,
96 and the 2.55 Ga Mount Owen batholith. The 2.62 Ga Wyoming batholith and Bears Ears granite
97 together represent the most extensive group of granite intrusions that contain abundant SPG: this
98 group of biotite granites extends from the Wind River Range across the Granite, Pedro, and
99 Shirley Mountains, and into the Laramie Mountains. Smaller bodies of SPG include the Rocky
100 Ridge garnet granite gneiss in the northern Laramie Mountains, and the Bear Mountain granite in
101 the Black Hills (Fig. 1). Geochemical data for these six suites is available in Online Material
102 Table OM1.

103 A plot of aluminum saturation index for samples from these suites (Fig 2a) shows that
104 they are overwhelmingly peraluminous. Most contain both weakly and strongly peraluminous
105 compositions, but the Rocky Ridge gneiss and Bear Mountain granite are entirely composed of
106 SPG. Two suites, the Webb Canyon gneiss and Bitch Creek gneiss, are calcic, whereas the others
107 are calc-alkalic to alkali-calcic (Fig. 2b). Most suites span the magnesian/ferroan boundary, but
108 the Webb Canyon gneiss is distinguished by strongly ferroan compositions (Fig 2c). On the basis
109 of these major element characteristics, the suites define three groups: calcic suites containing
110 SPG, calc-alkalic to alkali-calcic suites composed entirely of SPG, and calc-alkalic to alkali-calcic
111 suites composed of both weakly and strongly peraluminous rocks (Table 1). This subdivision

112 forms a basis for discussing the variety of sources and petrogenetic processes that produced

113 Archean SPG.

114 Table 1. Three types of Neoproterozoic SPG suites in the Wyoming Province.

SPG-bearing suite	Age (Ga)	Location	Geochemical classification (from Fig. 2)	Proportion of SPG
<i>Calcic suites</i>				
Webb Canyon gneiss	2.68	Teton Range	Calcic, ferroan, metaluminous to peraluminous	35%
Bitch Creek gneiss	2.68	Teton Range	Calcic, magnesian, peraluminous	38%
<i>Calc-alkalic to alkali-calcic suites composed entirely of strongly peraluminous granitic rocks</i>				
Bear Mt gneiss	2.59	Black Hills	Calc-alkalic to alkali-calcic, magnesian, strongly peraluminous	100%
Rocky Ridge garnet granite gneiss	2.64	Laramie Mts	Calc-alkalic to alkali-calcic, ferroan to magnesian, strongly peraluminous	100%
<i>Calc-alkalic to alkali-calcic suites with both weakly and strongly peraluminous granitic rocks</i>				
Mount Owen batholith	2.55	Teton Range	Calc-alkalic to alkali-calcic, ferroan to magnesian, peraluminous	33%
Wyoming batholith & Bears Ears granite	2.62	Granite, Laramie, Wind River Mts	Calc-alkalic to alkali-calcic, ferroan to magnesian, peraluminous	37%

115

116 **Calcic SPG suites**

117 The two calcic granitoid suites are located in the Teton Range. The calcic Webb Canyon

118 Gneiss and Bitch Creek Gneiss crop out in the northern portion of the small, 50 x 16 km area of

119 Archean outcrop exposed in the Teton Range (Frost et al., 2016).

120 **Webb Canyon Gneiss.** The Webb Canyon Gneiss is a weakly layered to massive leucogranitic
121 orthogneiss that is exposed as a series of elongate, sheet-like bodies approximately 2 km wide
122 and up to 10 km in length. It generally shows a strong foliation defined by biotite, particularly
123 intense adjacent to contacts with the Layered Gneiss it intrudes. Webb Canyon Gneiss is
124 generally fine-grained, with crystals typically less than 2 mm in their longest dimension. It
125 consists mainly of quartz and albitic plagioclase, along with 5-20% alkali feldspar. Depending on
126 the proportion of alkali feldspar, samples include both trondhjemite and granodiorite.
127 Hornblende and biotite are present in most samples, although samples from the eastern sheet lack
128 hornblende. Garnet is present in some samples and is subhedral to anhedral. Allanite, zircon,
129 titanite, apatite, and secondary epidote are common accessory minerals. Intergrown biotite and
130 oxide is interpreted to suggest that pyroxene was initially present in some samples (Frost et al.,
131 2016). U-Pb zircon age determinations of seven samples of Webb Canyon Gneiss vary from
132 2686 ± 5 Ma to 2674 ± 5 Ma (Frost et al., 2016).

133 **Bitch Creek Gneiss.** The Bitch Creek Gneiss occurs within the older Layered Gneiss of the
134 Teton Range as sill- or dike-like bodies typically 2-5 m wide and approximately 100 m long, and
135 small plutons up to 100 m across. In general, the Bitch Creek gneiss is lighter in color and
136 displays a weaker foliation than Webb Canyon Gneiss. It is trondhjemitic, containing quartz and
137 plagioclase, and almost no alkali feldspar. Biotite is the primary ferromagnesian mineral;
138 hornblende is absent. Garnet is poikilitic, strongly resorbed, and surrounded by a light-colored
139 halo in which biotite is absent. Zircon and allanite are less abundant than in Webb Canyon
140 Gneiss. U-Pb zircon age determinations of two samples of Bitch Creek Gneiss yielded 2686 ± 3
141 Ma and 2675 ± 6 Ma, identical within error to the range of ages for the Webb Canyon Gneiss
142 (Frost et al., 2016).

143

144 **Calc-alkalic to alkali-calcic suites composed entirely of strongly peraluminous granite**

145 The two suites that are entirely SPG are found in the eastern part of the Wyoming
146 Province, one in the northern Laramie Mountains (Da Prat, 2020) and the other in the Black Hills
147 (Gosselin et al., 1988; 1990).

148 **Rocky Ridge Garnet Granite Gneiss.** Muscovite garnet granite gneiss is exposed in the
149 northern Laramie Mountains, where it is one of the most extensive rock units, occupying an
150 outcrop area in excess of 25 km² (Da Prat, 2020). The gneiss is folded with amphibolite, granitic
151 gneiss, and various supracrustal rocks. It is composed of quartz, potassium feldspar, plagioclase,
152 garnet, and muscovite with minor biotite. Garnet is 0.1-4 cm and muscovite is <0.1-2 cm in size.
153 Accessory minerals include zircon, spinel, apatite, oxides, and titanite. Locally the unit is
154 sillimanite-bearing. The unit is strongly foliated. Leucocratic lenses, some garnet-bearing, and
155 biotite selvages in biotite ± muscovite schist and hornblende biotite granite gneiss adjacent to the
156 Rocky Ridge SPG are interpreted to suggest that the garnet granite gneiss was formed by partial
157 melting of these older units. Zircon in this unit is sparse, and typically complexly zoned,
158 metamict and altered, and contains high common Pb and high U contents. U-Pb analysis of five
159 samples revealed inherited zircon of ≥ 3 Ga in all samples. However, despite careful analysis of
160 the least altered areas, a crystallization age was not obtained (Da Prat, 2020). Rocky Ridge
161 Gneiss is constrained by field relations to be younger than 2.72 Ga hornblende biotite granite
162 gneiss and older than the ~2.64 Ga deformation event that produced the foliation in the Rocky
163 Ridge Gneiss.

164 **Bear Mountain granite.** The Bear Mountain granite is it exposed along the western flanks of the
165 Black Hills. It occurs as concordant, sill-like bodies of granite, trondhjemite, and granite

166 pegmatite within a well-foliated biotite-plagioclase schist. The granite is composed of quartz
167 (32-35%), plagioclase (23-32%), microcline (20-31%), and muscovite (2-14%). The
168 trondhjemite is composed of quartz (36-40%), plagioclase (26-29%), muscovite (15-22%), and
169 microcline (trace-4%). Accessory minerals in both rock types include garnet, biotite, and apatite
170 (Gosselin et al., 1988). Zircon crystals are highly metamict and altered but preserve local
171 unaltered areas that were dated by McCombs et al. (2004) at 2596 ± 11 Ma.

172

173 **Calc-alkalic to alkali-calcic suites containing both weakly and strongly peraluminous**
174 **granite**

175 Neoproterozoic granite occupies the majority of outcrop across the central Wyoming
176 Province, from the Wind River Range to the Laramie Mountains. In the Granite, Pedro, Shirley,
177 and Laramie Mountains this 2.62 Ga granite is known as the Wyoming batholith (Bagdonas et
178 al., 2016). In the Wind River Range, several intrusions of granite of the same age and
179 composition are collectively known as the Bears Ears granite (Stuckless, 1989). The
180 southernmost of these plutons is spatially associated with the calc-alkalic 2.63 Ga Louis Lake
181 batholith. Because they are the same age and are indistinguishable compositionally, we group the
182 Wyoming and Bears Ears granites and consider them a single suite of SPG. The other SPG suite
183 in this group, the Mount Owen batholith, is both younger (2.55 Ga) and much smaller (150
184 km²)(Frost et al., 2018) than the Wyoming batholith and Bears Ears granite.

185 **Mount Owen batholith.** The Mount Owen batholith, which intrudes the central Teton Range, is
186 an undeformed peraluminous leucogranite composed of quartz, alkali feldspar, plagioclase,
187 biotite and muscovite. In some rocks, the dominant mica is biotite and in others it is muscovite.
188 Garnet is present in some samples, and in others sillimanite needles are present in quartz. Zircon

189 is abundant, and allanite and monazite are present in some samples (Frost et al., 2018). The
190 grain-size of the granite is heterogeneous on the outcrop scale, suggesting that water activity was
191 highly variable during emplacement. Pegmatitic and aplitic dikes of Mount Owen affinity are
192 present throughout the range, extending many kilometers away from the main intrusion. Some
193 pegmatitic dikes contain tourmaline. The Mount Owen batholith was emplaced at 2547 ± 3 Ma
194 (Zartman and Reed, 1998).

195 **Wyoming batholith and Bears Ears granite.** The 2.62 Ga Wyoming batholith occupies
196 Archean exposures in the Granite, Pedro, Shirley, and Laramie Mountains (Bagdonas et al.,
197 2016). It is composed of two units: biotite granite and leucocratic banded granite. Homogeneous,
198 undeformed biotite granite occupies 90% of outcrops. It is a medium to coarse-grained unit
199 composed of microcline, quartz, plagioclase, and biotite. Accessory minerals include titanite,
200 magnetite, zircon, apatite, and secondary epidote. Trace amounts of muscovite are present in
201 some samples. Leucocratic banded granite makes up approximately 10% of outcrops and is
202 present across the Wyoming batholith. It appears to be more common along batholith margins
203 and near the roof of the batholith. Leucocratic banded granite is more quartz-rich than the biotite
204 granite and contains up to 5% magnetite. Compositional banding is defined by biotite and most
205 likely formed due to magmatic flow. Magnetite can be centimeters in diameter and appears to
206 have formed at the expense of biotite (Bagdonas et al., 2016). The roof of the batholith is most
207 extensively exposed in the northern Laramie Mountains, where it shallowly underlies older
208 schists and granitic gneisses (Da Prat, 2020). There the Wyoming batholith changes from
209 medium-grained and equigranular to coarse-grained and pegmatitic. Pegmatite contains
210 muscovite \pm garnet \pm tourmaline in addition to alkali feldspar, quartz, plagioclase, and biotite.

211 Pegmatite dikes and sills intrude the older gneisses above the contact with the Wyoming
212 batholith (Da Prat, 2020).

213 The type locality of the Bears Ears granite in the southern Wind River Mountains is
214 interpreted to be the youngest component of the calc-alkalic Louis Lake batholith (Frost et al.,
215 1998). It is an undeformed, equigranular to porphyritic biotite granite. In this locality, the
216 contacts with the slightly older granodiorite and quartz diorite rocks are gradational in places,
217 and in other places the Bears Ears granite crosscuts the older units. Two samples were dated at
218 2.62 Ga by Wall (2004), indistinguishable within error from two dates of the Wyoming batholith
219 by Bagdonas et al. (2016). In our data compilation, we include Bears Ears granite samples from
220 the type locality as well as samples from the New Fork Lakes and Middle Mountain areas of the
221 Wind River Range as part of the Bears Ears granite (Table OM-1). These are plotted together
222 with the Wyoming batholith data on figures 2-6.

223

224 **Geochemical characteristics of Wyoming Province SPG**

225 **Geochemistry of calcic suites**

226 Although the Webb Canyon and Bitch Creek gneisses are both calcic and only subtly
227 distinguishable in the field and in thin section, many aspects of their major and trace element
228 characteristics are quite different (Frost et al., 2016; Table OM1).

229 Webb Canyon Gneiss is silica-rich, with SiO₂ varying from 70-80%. Alumina contents
230 are relatively low, such that one third of the samples are metaluminous, another third only
231 weakly peraluminous, and the final third are strongly peraluminous (Fig 2a). Most samples are
232 strongly ferroan, apart from six samples from the eastern sheet that lack hornblende (Fig. 2c).
233 (These six samples have higher MgO and lower CaO and Sr than other Webb Canyon gneiss

234 samples.) K_2O/Na_2O is variable, reflecting variable modal alkali feldspar content (Fig. 3).

235 Al_2O_3/TiO_2 is low, primarily reflecting the low alumina content of these rocks (Fig. 4).

236 Compared to the Webb Canyon Gneiss, the Bitch Creek Gneiss has lower SiO_2 (64-75%)
237 and higher alumina than the Webb Canyon Gneiss. As a result, only the most mafic sample is
238 metaluminous (Fig. 2a). Bitch Creek Gneiss samples have low K_2O/Na_2O ratios, reflecting the
239 near-absence of alkali feldspar (Fig. 3). Most samples are magnesian (Fig. 2c). CaO/Na_2O is
240 high, reflecting the plagioclase-rich nature of these rocks, and Al_2O_3/TiO_2 is low due to the
241 relatively high TiO_2 contents of this unit (Fig. 4).

242 Trace element characteristics of Webb Canyon Gneiss also contrast with those for Bitch
243 Creek Gneiss. Zirconium is higher (240-830 ppm) in the Webb Canyon Gneiss and lower (70-
244 400 ppm) in the Bitch Creek Gneiss (Fig. 5). Neither gneiss contains significant inherited zircon
245 (Frost et al., 2016), thus zircon saturation temperatures of $>900^\circ C$ and $750-900^\circ C$ respectively
246 suggest that Webb Canyon Gneiss magmas were hotter than Bitch Creek Gneiss magmas. Sr
247 contents of the Webb Canyon Gneiss are relatively low, from 20 to 200 ppm, whereas Bitch
248 Creek gneisses have higher Sr contents averaging 300 ppm (Fig. 6). Similarly low Rb contents in
249 both sets of gneisses yield higher Rb/Sr in the Webb Canyon gneisses (Fig. 6). Ba varies from
250 100 to nearly 3500 ppm in the Webb Canyon gneiss, whereas Ba is less than 100 ppm in Bitch
251 Creek Gneiss. As a result, Webb Canyon Gneiss exhibits a large range in Sr/Ba compared to the
252 Bitch Creek Gneiss (Fig. 6b).

253 The Webb Canyon and Bitch Creek gneisses also have distinct rare earth characteristics
254 (Fig. 7a). The Webb Canyon Gneiss is REE-enriched. Patterns are relatively flat and most
255 samples have a deep negative Eu anomaly. Five Webb Canyon samples have slightly lower REE
256 contents and lack Eu anomalies. These samples contain abundant plagioclase and are higher in

257 CaO and lower in K₂O than other samples. REE abundances of Bitch Creek gneisses are lower,
258 Eu anomalies are modest and include both positive and negative anomalies, and patterns are
259 LREE-enriched and HREE-depleted (Fig. 7a). Both Webb Canyon and Bitch Creek gneisses
260 have positive initial ϵ_{Nd} isotopic compositions that are consistent with a common, relatively
261 juvenile source (Frost et al., 2016).

262 **Petrogenesis of calcic SPG.** Frost et al. (2016) noted that the different roles of plagioclase and
263 hornblende can explain the different geochemical characteristics of the two different calcic SPG
264 suites in the Teton Range. High Sr and alumina in the Bitch Creek Gneiss likely reflects that
265 melting of plagioclase played a role in the formation of that magma. On the other hand, lower Sr
266 and alumina in the Webb Canyon Gneiss samples, along with negative Eu anomalies, indicate
267 plagioclase fractionation or retention in the source. High Y and REE contents may indicate the
268 melting of hornblende or garnet in the production of Webb Canyon magmas.

269 Experimental studies help to identify the sources and petrogenetic processes that may be
270 responsible for the two types of calcic SPG-bearing suites. Beard and Lofgren (1991) conducted
271 partial melting experiments on greenstone and amphibolite from the Jurassic Smartville complex
272 of California at 850-1000°C and pressures up to 6.9 kb. Although the partial melts obtained in
273 water-excess and dehydration melting experiments were both strongly calcic, in other respects
274 they were quite different (Fig. 8a-c). In the water-excess experiments, plagioclase broke down,
275 yielding an amphibole-rich restite and a strongly peraluminous melt. In the dehydration melting
276 experiments, quartz and amphibole broke down to produce pyroxenes in the restite and mildly
277 peraluminous to metaluminous granodioritic and trondhjemite melts. These experiments suggest
278 that water-excess melting by the reaction $hb + pl + qz + vapor = melt$, in which plagioclase
279 breaks down leaving an amphibole-rich restite, should produce magmas higher in alumina and

280 lower in FeO, along with higher Sr and depleted HREEs, all characteristics observed in Bitch
281 Creek gneisses. By contrast, dehydration melting involving breakdown of amphibole and quartz
282 by the reaction $hb + qz = pl + opx + cpx + melt$ can account for the low alumina, high FeO^t, high
283 silica content and trace element characteristics of the Webb Canyon gneiss. The water-excess
284 melting that produces the Bitch Creek gneiss composition takes place at lower temperature than
285 the dehydration reaction that generates the Webb Canyon gneiss composition, as is also
286 suggested by the lower zircon-saturation temperatures of the Bitch Creek Gneiss (Figs. 5, 9).

287 **Tectonic implications.** The Neoproterozoic rocks of the northern Teton Range have been
288 interpreted to record lateral, collisional orogeny. Mafic and metapelitic rocks were tectonically
289 buried to depths of >12 kb and reached temperatures of >900°C at 2695 Ma. This crust was
290 exhumed and juxtaposed with juvenile metasediments and mafic rocks at 2685 Ma (Swapp et al.,
291 2018). Shortly thereafter and for as long as 10 million years following, Webb Canyon and Bitch
292 Creek leucogranites that formed by dehydration melting and water-excess melting were
293 emplaced (Frost et al., 2016). This history is analogous to Cenozoic continental collisions such
294 as the Alps or Himalayas (Swapp et al., 2018).

295 Calcic peraluminous magmas in collisional environments may form by either water-
296 excess melting or dehydration melting of hb-pl-bearing rocks. Water-excess melting may occur
297 when relatively cool and hydrous rocks are thrust under hotter rocks. The water released from the
298 lower plate invades the hotter upper plate, inducing melting. Dehydration melts are likely to
299 occur when dramatically overthickened crust undergoes gravitational collapse and tectonic
300 extension, and partial melting takes place in response to decompression (Frost et al., 2016).

301

302 **Geochemistry of suites that are entirely composed of SPG**

303 The Rocky Ridge and Bear Mountain suites include the most strongly peraluminous
304 granitic rocks of the Wyoming Province, with all samples having $ASI > 1.1$. Samples from both
305 suites are characterized by very low Zr and TiO_2 contents.

306 **Rocky Ridge garnet granite gneiss.** Although all Rocky Ridge garnet granite gneiss samples
307 are strongly peraluminous, the suite includes samples with a range of major and trace element
308 characteristics. Silica ranges from 72 to 78% SiO_2 with one outlier at 68% SiO_2 , and
309 compositions vary from ferroan to magnesian, and calc-alkalic to alkali-calcic (Fig. 2).
310 K_2O/Na_2O varies from 0.3 to 2.5 (Fig. 3). CaO/Na_2O is variable, and Al_2O_3/TiO_2 are variable but
311 generally high due to low TiO_2 contents (Fig. 4).

312 Zr contents of Rocky Ridge garnet granite gneiss are very low (12-110 ppm; Fig. 5). The
313 sparse zircon in this unit is overwhelmingly dominated by inherited grains (Da Prat, 2020) and
314 therefore calculated zircon saturation temperatures based on observed Zr contents overestimate
315 magmatic temperatures. Rb/Ba and Rb/Sr ratios are variable but include the highest ratios of all
316 Wyoming Neoproterozoic SPG. Sr, Ba, and Y contents are low. REE patterns tend to be LREE-
317 enriched with variable, positive to negative Eu anomalies (Fig. 7). HREE contents vary and are
318 highest in the samples with the most garnet.

319 **Bear Mountain granite.** The Bear Mountain granite, like the Rocky Ridge garnet granite gneiss,
320 is entirely composed of strongly peraluminous rocks (Fig. 2a). The suite includes both
321 trondhjemites, which are magnesian, and granites, which are magnesian to ferroan (Fig. 2c). All
322 samples have similar silica and alumina contents and low CaO. The trondhjemite samples are
323 calc-alkalic to calcic and have low K_2O , whereas and the granite samples are alkali-calcic to
324 alkalic and have higher K_2O (Fig 2bc, 3). These geochemical differences reflect variations in the

325 modal abundance of alkali feldspar and muscovite in these rock types. CaO/Na₂O is low and
326 Al₂O₃/TiO₂ is high due to low TiO₂ (Fig. 4).

327 Zr contents are very low (5-80 ppm) and yield zircon saturation temperatures of 550-
328 800°C (Fig. 5). Rb/Ba, Rb/Sr, and Sr/Ba are high (Fig. 6). Y and REE abundances are low. REE
329 patterns for trondhjemite are lower and flatter than patterns for granite. Eu anomalies are mostly
330 pronounced and negative but two are slightly positive (Fig. 7). Sr and Eu contents are strongly
331 correlated (Gosselin et al., 1990).

332 **Interpretation of suites that are entirely SPG.** Field relations between SPG and micaceous
333 schists led Da Prat (2020) and Gosselin et al. (1990) to suggest that the Rocky Ridge and Bear
334 Mountain SPG formed by partial melting of metasedimentary rocks. The uniformly siliceous and
335 strongly peraluminous nature of these gneisses is compatible with this hypothesis. Although it is
336 possible to produce peraluminous residual melts by fractionation of aluminum-poor phases such
337 as hornblende or pyroxene from metaluminous magma (Cawthorn and Brown, 1976; Zen, 1986),
338 and marginally peraluminous melts can be driven to more peraluminous compositions by
339 fractionation of feldspars (Clarke, 2019), these processes are more likely to result in rocks with a
340 range of silica contents and weakly peraluminous ASI rather than strongly peraluminous
341 leucogranites.

342 Geochemical characteristics of these rocks are best explained by anatexis of a
343 metasedimentary source. Experimental data show that melting of muscovite-bearing metapelitic
344 schist can produce SPG that vary from magnesian to ferroan, and that are calc-alkalic to alkali-
345 calcic (Fig. 8d-f), similar to the characteristics observed in Bear Mountain and Rocky Ridge
346 granites. Compared to other Neoproterozoic SPG in the Wyoming Province, the Bear Mountain and
347 Rocky Ridge granites are distinguished by very low Zr contents and variable but low zircon

348 saturation temperatures (550-800°C)(Fig. 5). As noted above, these units contain sparse,
349 complexly zoned and mottled zircon. In the Rocky Ridge gneiss, the U-Pb systematics of these
350 zircon indicate that they are older, inherited grains. Including Zr held in these grains in the zircon
351 saturation temperature calculation yields temperatures that are too high. Da Prat (2020)
352 concluded that the temperature determination of 670-690°C obtained using metamorphic
353 assemblage diagrams is a better estimate of magma temperature.

354 Low magma temperatures are consistent with the low TiO₂ and Ba contents and high
355 Al₂O₃/TiO₂ of the Bear Mountain and Rocky Ridge granites (Table OM1, Fig. 5). Ti and Ba are
356 compatible in biotite, and their low abundances in the SPG gneisses suggest that biotite was not
357 involved in the melting reactions. Biotite dehydration melting takes place at temperatures above
358 720°C (Le Breton and Thompson, 1988), higher than the temperature calculated for Rocky Ridge
359 gneiss. We therefore suggest that the melt-forming reaction for these SPG rocks involved
360 melting of muscovite in a metasedimentary source.

361 The Bear Mountain and Rocky Ridge SPG also tend to have low calcium relative to
362 sodium, with most samples CaO/Na₂O < 0.2. Low ratios can indicate a clay-rich source: partial
363 melting experiments have shown that during vapor-absent melting of plagioclase-poor pelitic
364 rock, sodium entered the melt but calcium was retained in residual garnet, yielding melts with
365 CaO/Na₂O of 0.1 - 0.3 (Fig. 10a; Castro et al., 1999; Patino Douce and Harris, 1998; Pickering
366 and Johnston, 1998). The slightly higher CaO/Na₂O of some Bear Mountain and Rocky Ridge
367 SPG might be due to more plagioclase-rich source rocks: experiments with such starting
368 compositions gave melts with higher CaO/Na₂O (Fig 10b). Or, the higher ratios may be
369 attributable to vapor-present melting, which has been shown to lead to more extensive melting of
370 plagioclase and higher CaO/Na₂O in the melt (Holtz and Johannes, 1991).

371 The ratios of Rb, Sr, and Ba, which are held mainly in micas and feldspars, differ in Bear
372 Mountain and Rocky Ridge SPG. Rocky Ridge samples have low Sr/Ba (especially for samples
373 with low CaO/Na₂O) and high Rb/Ba and Rb/Sr. By contrast, Bear Mountain samples are
374 distinguished by high Sr/Ba, especially for trondhjemites, high Rb/Ba, and somewhat lower
375 average Rb/Sr. Low Sr/Ba in Rocky Ridge samples may indicate retention of plagioclase in the
376 restite, as is expected for vapor-absent muscovite dehydration melting because little melt is
377 produced (Harris and Inger, 1992). High Sr/Ba in Bear Mountain, particularly for the
378 trondhjemites, likely indicates greater consumption of plagioclase during vapor-present melting,
379 a process that would also produce their observed high Na₂O/K₂O (Fig. 3) (Castro et al., 1999;
380 Patiño Douce and Harris, 1998). Interpretation of the other ratios is less definitive. High Rb/Ba
381 and Rb/Sr, when coupled with low CaO/Na₂O, may indicate a clay-rich source (Harris and Inger,
382 1992). However, ratios of Rb/Ba and Rb/Sr in the melt also depend upon the amount of residual
383 plagioclase and K-feldspar. Knowledge of the abundances of these elements in the magma
384 sources as well as the residual mineralogy of the partial melting reactions would be needed to
385 distinguish these alternatives (Nabelek, 2020).

386 Rocky Ridge and Bear Mountain granites have the lowest REE contents of any of the
387 Wyoming Neoproterozoic SPG (Fig. 7b). This may reflect the retention of REE-bearing accessory
388 minerals like zircon and monazite in the source during low-temperature anatexis, as was
389 suggested for the Proterozoic Harney Peak SPG in the Black Hills, South Dakota (Nabelek and
390 Glascock, 1995).

391 **Tectonic implications.** Strongly peraluminous granite intrusions formed by low-temperature
392 anatectic melting of metasedimentary rocks are commonly found within collisional orogens
393 (Sylvester, 1998). Sedimentary rocks are overridden during continent-continent collision. The

394 collision results in crustal thickening accompanied by heating of the sedimentary sequence,
395 followed by gravitational collapse. Partial melting may occur when deeply buried
396 metasedimentary rocks intersect muscovite dehydration melting reactions during decompression,
397 producing SPG melts. Other mechanisms such as flux melting also may result in SPG anatexis
398 and magma production in collisional orogens (Nabelek, 2020), and may have contributed to the
399 formation of some Bear Mountain SPG, especially the trondhjemites.

400

401 **Calc-alkalic to alkali-calcic suites with both weakly and strongly peraluminous granite**

402 The Mount Owen batholith is a peraluminous leucogranite with a limited range of silica
403 contents ($\text{SiO}_2 = 73.7\%$ to 75.7% , plus one sample with 71.6%). One-third of the samples are
404 strongly peraluminous; these tend to be alkali-calcic whereas weakly peraluminous samples are
405 calc-alkalic (Fig. 2ab). Samples vary from ferroan to magnesian, with strongly peraluminous
406 samples tending to be magnesian (Fig. 2c). The strongly peraluminous samples have $\text{K}_2\text{O} > \text{Na}_2\text{O}$
407 (Fig. 3). They have lower $\text{CaO}/\text{Na}_2\text{O}$, $\text{Al}_2\text{O}_3/\text{TiO}_2$, and Zr abundances than the weakly
408 peraluminous samples (Figs. 4, 5). Mount Owen leucogranite has high Rb/Ba and Rb/Sr and low
409 Sr/Ba, similar to the Rocky Ridge SPG (Fig. 6).

410 Wyoming batholith and Bears Ears granite group of samples exhibit a larger range of
411 silica ($\text{SiO}_2 = 70.2\%$ to 77.1%) than do Mount Owen batholith samples. Like the Mount Owen
412 batholith, the strongly peraluminous samples of the Wyoming batholith and Bears Ears granite
413 are more alkali-calcic on average than the weakly peraluminous samples (Fig. 2ab). Both
414 strongly and weakly peraluminous samples span the ferroan-magnesian boundary (Fig. 2c) and
415 both have $\text{K}_2\text{O} > \text{Na}_2\text{O}$ (Fig. 3). $\text{Al}_2\text{O}_3/\text{TiO}_2$ is relatively low except for pegmatitic samples from
416 the roof zone of the Wyoming batholith in the northern Laramie Mountains (Fig. 4). Both

417 CaO/Na₂O and Zr are quite variable (Figs. 4, 5). Zr contents and zircon saturation temperatures
418 are higher than for the Mount Owen batholith (Fig. 5). Rb/Ba, Rb/Sr and Sr/Ba are intermediate
419 between the calcic and entirely SPG suites (Fig. 6ab).

420 Mount Owen granites are LREE-enriched with negative Eu anomalies, but less strongly
421 LREE-enriched than the Bears Ears and Wyoming batholith (Fig. 7cd). With the exception of
422 samples from the pegmatitic roof zone to the Wyoming batholith, which share the geochemical
423 characteristics of the the entirely SPG suites, Wyoming batholith granites exhibit LREE-enriched
424 patterns with deep negative Eu anomalies. The Bears Ears granites have similar LREE-enriched
425 patterns, although several samples with the lowest REE have positive Eu anomalies suggesting
426 feldspar accumulation (Fig. 7d). LREE abundances of the Wyoming batholith and Bears Ears
427 granite are higher than for any other suite except for the calcic Webb Canyon gneiss. Four
428 pegmatite samples from the northern Laramie Mountains have flatter patterns and lower REE
429 contents than the biotite granite that makes up the majority of the batholith (Fig. 7d).

430 **Interpretation of suites containing weakly and strongly peraluminous granitic rocks.**

431 Although the Mount Owen and the Wyoming batholith suites share some similarities, including
432 both weakly and strongly peraluminous granitic rocks and overlapping MALI, Fe-indices, and
433 K₂O/Na₂O (Figs. 2bc, 3), other features suggest they originated from different sources and
434 petrogenetic processes. The smaller 2.55 Ga Mount Owen batholith intrudes older Neoproterozoic
435 Layered Gneiss that is composed of quartzofeldspathic gneiss, metagraywacke, and amphibolite
436 (Frost et al., 2018). Calculated zircon saturation temperatures for the Mount Owen batholith of
437 690-870°C are higher than those estimated for the Rocky Ridge SPG gneiss (670-690°C; Da
438 Prat, 2020). Its lower Al₂O₃/TiO₂ compared to the solely SPG suites also suggests higher magma
439 temperatures and the involvement of biotite in melting reactions. Higher CaO/Na₂O compared to

440 the entirely SPG suites is consistent with a more plagioclase-rich source (Fig. 10), and the initial
441 Nd isotopic compositions of the Mount Owen batholith are within the range of the initial Nd
442 isotopic compositions of the Layered Gneiss (Frost et al., 2006a; 2016). Taken together, these
443 characteristics suggest breakdown of biotite during partial melting of graywacke and/or
444 quartzofeldspathic gneiss by a reaction such as $bt + q + pl = opx + orthoclase$ component of
445 plagioclase + gar + melt (Vielzeuf and Montel, 1994). In other words, the Mount Owen
446 batholith, and Rocky Ridge and Bear Mountain SPG all formed by crustal melting, but the
447 Mount Owen source rock was more biotite- and plagioclase-rich.

448 The Wyoming batholith and Bears Ears granite are by far the most voluminous of the
449 Neoproterozoic SPG suites in the Wyoming Province. Field relations suggest that Bears Ears granite
450 is closely related to the 2.63 Ga Louis Lake batholith, a continental arc batholith that occupies
451 the southern half of the Wind River Range (Frost et al., 1998). Geochemical and isotopic data are
452 consistent with formation of the Bears Ears granite by differentiation from Louis Lake
453 granodiorites (Bagdonas et al., 2016). The Bears Ears granite is geochemically indistinguishable
454 from the Wyoming batholith, which led Bagdonas et al. (2016) to suggest that similar magma
455 sources supplied all the 2.62 Ga granites. This hypothesis implies that the subduction-related
456 input of mantle-derived heat and magma was widespread across the southern Wyoming
457 Province.

458 Initial Nd isotopic compositions show that although Louis Lake and Bears Ears samples
459 have overlapping initial ϵ_{Nd} , many Wyoming batholith samples have more negative initial ϵ_{Nd}
460 indicating that they have either assimilated greater proportions of crust or were contaminated by
461 older, less radiogenic Archean crust (Fig. 11). The initial ϵ_{Nd} of the strongly peraluminous
462 samples (-3.0) are on average more negative than the weakly peraluminous samples (-1.6),

463 suggesting that assimilation of aluminous crustal melts enhanced the peraluminous nature of the
464 granite magmas. There is a general trend of increasing ASI and decreasing initial ϵ_{Nd} from west
465 to east (Fig. 12). This trend suggests that the crustal assimilant involved in producing the
466 magmas is more aluminous in the eastern Wyoming Province. The fact that the Rocky Ridge and
467 Bear Mountain SPG are found in this part of the province supports such a hypothesis.

468 The pegmatitic dikes and sills that form the roof of the Wyoming batholith in the
469 northern Laramie Mountains are both mineralogically and chemically distinct from the main
470 intrusion. They exhibit variable grain sizes and are commonly muscovite-, garnet-, and locally
471 tourmaline-bearing. The Al_2O_3/TiO_2 ratios and trace element compositions of these pegmatitic
472 rocks are similar to Rocky Ridge SPG gneiss, suggesting that they formed by partial melting of
473 aluminous crust in response to heating by Wyoming batholith magma (Figs. 5, 6).

474 **Tectonic implications.** Although both the Mount Owen and the Wyoming batholith calc-alkalic
475 to alkali-calcic leucogranite suites contain crustal components, the processes by which they
476 formed are likely to have been different. The Mount Owen batholith most likely formed by
477 crustal melting of a biotite- and plagioclase-bearing metasedimentary rock and/or
478 quartzofeldspathic orthogneiss. In contrast, the Wyoming batholith and Bears Ears granite
479 formed by fractionation of calc-alkaline continental arc magmas, accompanied by assimilation of
480 felsic crust.

481

482 **Discussion: Petrogenesis of Neoproterozoic SPG in the Wyoming Province**

483 The three groups of Neoproterozoic SPG of the Wyoming Province are compositionally
484 distinct and were produced by different petrologic processes, all of which also occur in the
485 Phanerozoic.

486 The calcic SPG are best explained by partial melting of hornblende-plagioclase rocks: the
487 Webb Canyon suite formed by dehydration melting and the Bitch Creek suite by water-excess
488 melting. These processes formed trondhjemites with distinctively different major and trace
489 element compositions. Phanerozoic examples of peraluminous trondhjemites formed by partial
490 melting of mafic rocks include the type locality trondhjemites of Trondheim, Norway (Slagstad,
491 2003), trondhjemites of the Smartville Complex, California (Beard and Lofgren, 1991),
492 trondhjemite dikes in the Blue Ridge Mountains of North Carolina and Georgia (Wood and
493 Miller, 1984), and tonalites and trondhjemites of the Cornucopia Stock of northeastern Oregon
494 (Johnson et al., 1997). The continent-continent collision responsible for the Webb Canyon and
495 Bitch Creek gneisses, in which underthrusting and crustal thickening was followed by
496 gravitational collapse (Swapp et al., 2018) is analogous to Neogene Himalayan collisional
497 processes. The reason that the Archean intrusions are calcic trondhjemites whereas the modern
498 Himalayan leucogranites are true granites is related to the fundamental difference in the
499 composition of the crust in the Tetons and the Himalayas. The crust that partially melted in the
500 Tetons was composed of greywacke, tonalite, and amphibolite. These rocks, which are less
501 potassic than the pelitic sources of the Himalayan leucogranites, also required higher
502 temperatures to partially melt than were required to partially melt the pelitic rocks in the
503 Himalayas (Frost et al., 2016). However, compositional differences aside, the Webb Canyon and
504 Bitch Creek SPG are evidence that the same general processes of melt formation, migration and
505 solidification have taken place in collisional orogens for at least 2.7 Ga.

506 The petrogenesis of several of the Wyoming SPG suites appears to involve anatexis of
507 metasedimentary rocks. The Rocky Ridge and Bear Mountain suites bear the hallmarks of
508 leucogranitic rocks formed by partial melting of pelitic rocks by reactions involving muscovite.

509 As such, they are compositionally analogous to other ancient and modern collisional
510 leucogranites formed from metamorphosed, deformed, and partially-melted pelitic rocks
511 including in the Proterozoic Black Hills orogen, the Paleozoic Appalachian orogen, and the
512 Tertiary Himalayan orogen (Nabelek, 2020). The implication is that by 2.6 Ga in the eastern
513 Wyoming Province, processes of erosion and sedimentary recycling had produced aluminous,
514 fine-grained, clastic sedimentary rocks and that these were buried and heated to produce partial
515 melts. On the western side of the Wyoming Province, the 2.55 Ga Mount Owen batholith appears
516 to have formed from more plagioclase-rich crustal sources such as greywacke, by higher-
517 temperature melting reactions involving biotite, suggesting that in this part of the province
518 muscovite-bearing pelitic sources were minor or absent.

519 The other SPG-forming mechanism that appears to have operated during the Neoproterozoic
520 in the Wyoming Province is differentiation of continental arc magmas, accompanied by varying
521 amounts of crustal assimilation. This mechanism, which was responsible for the Wyoming
522 batholith and Bears Ears granite, produced far more true granite and strongly peraluminous
523 granite than is typical of Phanerozoic continental arcs. Bagdonas et al. (2016) suggested that the
524 Wyoming batholith represents the plutonic portion of a large rhyolitic system associated with a
525 continental arc, analogous to modern, shallow silicic batholiths that supply rhyolite calderas in
526 the central Andes. The large proportion of granite observed in the Wyoming continental arc
527 system may have formed in response to greater radioactive heat production and mantle power
528 input to the base of the crust in the late Archean, driving more extensive differentiation and
529 assimilation, and forming larger volumes of silicic magma compared to the modern day. The
530 significance of the continental arc setting for these SPG is that this plate tectonic process must
531 have been in place by the Neoproterozoic.

532 A summary of the defining characteristics of the Wyoming Neoproterozoic SPG and their
 533 interpretation (Table 2) indicates that plate tectonic processes of continent-continent collision
 534 and formation of magmatic arcs on evolved continental margins were established in the
 535 Wyoming Province by 2.68-2.60 Ga.

536

537 Table 2. Petrogenetic interpretation and tectonic significance of Wyoming Province SPG

SPG Suite and example	Geochemical characteristics	Petrogenetic interpretation	Tectonic significance
Calcic Webb Canyon Gneiss Bitch Creek gneiss	Calcic, low Al ₂ O ₃ /TiO ₂ and low Rb/Ba, high REE and Zr contents	Partial melting of hb-pl-bearing sources, by dehydration melting (Webb Canyon) or water-excess melting (Bitch Creek)	Collisional orogeny involving partial melting of relatively mafic sources such as tonalite, amphibolite, and graywacke
Alkalic-calcic to calc-alkalic, entirely SPG Rocky Ridge granite gneiss Bear Mountain granite Dikes and sills along roof zone of Wyoming batholith	ASI = 1.1-1.4 and higher, high Al ₂ O ₃ /TiO ₂ (due to low TiO ₂) and high Rb/Ba, low REE and Zr contents, low CaO/Na ₂ O	Partial melting of ms-bearing sources. Dehydration and water-excess melting; latter forms trondhjemites	Collisional orogeny involving partial melting of metapelitic sources. (Note these SPG also form by partial melting of aluminous crust in response to magmatic heating, as in the roof zone of the Wyoming batholith.)
Alkalic-calcic to calc-alkalic, weakly and strongly peraluminous Mount Owen batholith Wyoming batholith and Bears Ears granite	Intermediate to high CaO/Na ₂ O, K ₂ O/Na ₂ O, Rb/Ba, Zr and REE; intermediate to low Al ₂ O ₃ /TiO ₂	Partial melting reactions involving biotite (Mount Owen), or differentiation and crustal assimilation by calc-alkalic magmas	Collisional orogeny involving partial melting of bt-rich sources, such as graywacke (Mount Owen), or subduction-related continental arc magmatism (Wyoming batholith and Bears Ears granite)

538

539 **Implications for crustal evolution**

540 Various geochemical indicators suggest that the continental crust became more felsic in
541 the Neoproterozoic (e.g., Chen et al., 2020; Dhuime et al., 2015; Tang et al., 2016). Such a change in
542 composition will be reflected in the sedimentary rock record: erosion of K-rich granitic crust
543 followed by multiple cycles of weathering, transport, and deposition produces shale with a
544 characteristic geochemical composition (Taylor and McLennan, 1985). Subsequent burial and
545 metamorphism of shale produces metapelite, that when partially melted, forms SPG. Therefore,
546 the appearance in the rock record of SPG that formed by partial melting of metapelitic rocks is
547 powerful confirmation of this evolution in the composition of the Earth's crust.

548 This geochemical shift was not synchronous, either on local or global scales. The results
549 of this study indicate that the crustal sources to the SPG examined in this study vary across the
550 Wyoming Province, from more plagioclase-rich sources with more radiogenic Nd isotopic
551 compositions in the west and more felsic, potassic crust with less radiogenic Nd isotopic
552 compositions in the east (Fig. 12). Given that Archean cratons are commonly composed of
553 subprovinces with distinct geologic histories, it is not surprising that the age and composition of
554 the crust should vary spatially across a given province.

555 Worldwide, SPG interpreted to have formed by partial melting of metasedimentary rocks
556 appear in the rock record at different times on different cratons. In their review, Bucholz and
557 Spencer (2019) identified two Mesoproterozoic suites that include some SPG: the ~3.07 Ga Sinceni
558 intrusion and other latest Mesoproterozoic two-mica granites that intrude the Pongola Supergroup in
559 the Kaapvaal craton, and the 3067 Ma Annandagstoppane granite that is exposed in a very small
560 area of the Grunehogna craton of East Antarctica. However, most SPG formed later. They appear
561 on at least four different Archean cratons in the Neoproterozoic: in the Superior province (2.68-2.66

562 Ga), in Wyoming (>2.64-2.60 Ga), Slave (2.61-2.59 Ga), and Yilgarn (2.63-2.63 Ga) (Bucholz
563 and Spencer, 2019; this study). In these Archean provinces, the intrusion of SPG are among the
564 final events prior to cratonization, that is, the time after which they experience no penetrative
565 deformation and calc-alkalic magmatism and deformation. Other Archean provinces cratonized
566 later and the oldest SPG in those cratons also formed later. For example, in the North China
567 Craton, SPG appear at between 1.90-1.93 Ga, immediately followed by final Paleoproterozoic
568 assembly of the Western Block of the craton (Bucholz and Spencer, 2019; Zhao et al., 2005).

569 The global “bloom” of Neoproterozoic SPG follows the emergence of continental arcs above
570 subduction zones at the end of the Mesoproterozoic (Brown and Johnson, 2018), and coincides with
571 the assembly of the first supercontinents (Campbell and Allen, 2008). Both subduction beneath a
572 continental plate margin and amalgamation of crustal blocks by collisional orogeny provide
573 tectonic environments that transport sedimentary rocks to depths where partial melting occurs.
574 SPG record both of these environments in the Wyoming Province. Subduction beneath a
575 continental arc at 2.62 Ga is recorded by the Wyoming batholith and Bears Ears granite. The
576 remaining SPG record collisional orogenies occurring around the edges of the Wyoming
577 Province. The collisions at 2.68 Ga and 2.55 Ga in the Tetons are incompletely understood
578 because subsequent Proterozoic orogenies along the western and northern margins of the
579 Wyoming Province have removed much of the evidence. In southern Wyoming the ~2.64 Ga
580 Rocky Ridge SPG was intruded then deformed at the time when accreted terrains docked along
581 the southern margin of the province (Fig. 1)(Frost et al., 2006b), and the 2.60 Ga Bear Mountain
582 SPG formed at the same time as monazite and hydrothermal zircon growth (Bagdonas et al.,
583 2016; Vincent, 2017). These events may be related to the collision of Wyoming and Superior
584 provinces to create Neoproterozoic-Paleoproterozoic supercontinent Superia, a supercontinent that

585 rifted apart at ~2480 Ma and was rejoined along the Trans-Hudson orogen at ~1760 Ma (Dahl et
586 al., 2006; Davey et al., 2020; Ernst and Bleeker, 2010; Redden et al., 1990; Van Boening and
587 Nabelek, 2008).

588 In summary, the appearance of SPG in the Neoproterozoic rock record coincides with the
589 time when the continental crust became strong, thick, and evolved enough to support large,
590 elevated continental landmasses (Kump and Barley, 2007). Weathering and erosion of this
591 subaerial crust enabled the production and deposition of fine-grained, aluminous sediment
592 sources that are parental to many SPG. The establishment of strong crustal blocks also enabled
593 modern plate tectonic processes of subduction and continental collision, which take sedimentary
594 rocks from the Earth's surface to depth where they are metamorphosed and partially melted to
595 form SPG. Amalgamation of cratons by collisional orogenesis formed the Earth's first
596 supercontinents, an evolutionary development recorded by formation and emplacement of
597 voluminous SPG.

598

599 **Acknowledgements**

600 CDF thanks the officers, staff, and members of the Mineralogical Society of America for a
601 rewarding year as its 101st president. CDF and FDP acknowledge USGS EDMAP award number
602 G19AC0014 supporting geologic mapping and study of the Rocky Ridge gneiss as part of FDP's
603 M.S. thesis at the University of Wyoming. The authors thank C. Bucholz, B.R. Frost, and P.
604 Nabelek for their very helpful reviews.

605

606
607
608
609
610
611
612
613
614
615
616
617
618
619
620
621
622
623
624
625
626
627

References

Bagdonas, D.A., Frost, C.D., and Fanning, C.M. (2016) The Neoproterozoic Wyoming Batholith: a voluminous, homogeneous granite inboard of a continental arc. *American Mineralogist*, 101, 1332–1347.

Beard, J.S., and Lofgren, G.E. (1991) Dehydration melting and water-saturated melting of basaltic and andesitic greenstones and amphibolites at 1, 3, and 6.9 kb. *Journal of Petrology*, 32, 365–401.

Boehnke, P., Watson, E.B., Trail, D., Harrison, T.M., and Schmitt, A.K. (2013) Zircon saturation re-revisited. *Chemical Geology*, 351, 324–334.

Brown, K.L., Hart, W.K., and Stuck, R.J. (2018) Temporal and geochemical signatures in granitoids of northwestern Nevada: evidence for the continuity of the Mesozoic magmatic arc through the western Great Basin. *Lithosphere*, 10, 327–350.

Brown, M., and Johnson, T. (2018) Secular change in metamorphism and the onset of global plate tectonics. *American Mineralogist*, 103, 181–196.

Bucholz, C.E., and Spencer, C.J. (2019) Strongly peraluminous granites across the Archean-Proterozoic transition. *Journal of Petrology*, 60, 1299–1348.

Campbell, I.H., and Allen, C.M. (2008) Formation of supercontinents linked to increases in atmospheric oxygen. *Nature Geoscience*, 1, 554–558.

Castro, A., Patiño Douce A. E., Corretge, L.G., de la Rosa, J.D., El-Biad, M., El-Hmidi, H. (1999) Origin of peraluminous granites and granodiorites, Iberian massif, Spain: an experimental test of granite petrogenesis. *Contributions to Mineralogy and Petrology*, 135, 255–276.

- 628 Cawthorn, R.G. and Brown, P.A. (1976) A model for the formation and crystallization of
629 corundum-normative calc-alkaline magmas through amphibole fractionation. *Journal of*
630 *Geology*, 84, 467-476.
- 631 Chappell, B.W., and White, A.J.R. (2001) Two contrasting granite types: 25 years later.
632 *Australian Journal of Earth Sciences*, 48, 489–499.
- 633 Chen, K., Rudnick, R.L., Wang, Z. (2020) How mafic was the Archean upper continental crust?
634 Insights from Cu and Ag in ancient glacial diamictites. *Geochimica et Cosmochimica*
635 *Acta*, 278, 16–29.
- 636 Clarke, D.B. (2019) The origins of strongly peraluminous granitoid rocks. *The Canadian*
637 *Mineralogist*, 57, 529–550.
- 638 Conrad, W.K., Nicholls, I.A., and Wall, V.J., 1988, Water-saturated and -undersaturated melting
639 of metaluminous and peraluminous crustal compositions at 10 kb: evidence for the origin
640 of silicic magmas in the Taupo Volcanic Zone, New Zealand, and other occurrences:
641 *Journal of Petrology*, v. 29, p. 765-803.
- 642 Cornia, M.E. (2003) The Archean history of the Teton Range and surrounding areas. M.S. thesis,
643 University of Wyoming, Laramie.
- 644 Dahl, P.S., Hamilton, M.A., Wooden, J.L., Foland, K.A., Frei, R., McCombs, J.A., Holm, D.K.
645 (2006) 2480 Ma mafic magmatism in the northern Black Hills, South Dakota: a new link
646 connecting the Wyoming and Superior cratons. *Canadian Journal of Earth Sciences*, 43,
647 1579-1600.
- 648 Da Prat, F.A. (2020) Archean history of the northern Laramie Mountains. M.S. thesis, University
649 of Wyoming, Laramie.
- 650 Davey, S.C., Bleeker, W., Kamo, S.L., Vuollo, J., Ernst, R.E., and Cousens, B.L. (2020) Archean
651 block rotation in Western Karelia: resolving dyke swarm patterns in metacraton Karelia-

- 652 Kola for a refined paleogeographic reconstruction of supercraton Superia. *Lithos*, 368-
653 369, 105553.
- 654 Dhuime, B., Wuestefeld, A., and Hawkesworth, C.J. (2015) Emergence of modern continental
655 crust about 3 billion years ago. *Nature Geoscience*, 8, 552–555.
- 656 Ernst, R., and Bleeker, W. (2010) Large igneous provinces (LIPs), giant dike swarms, and
657 mantle plumes: significance for breakup events within Canada and adjacent regions from
658 2.5 Ga to the present. *Canadian Journal of Earth Sciences*, 47, 695–739.
- 659 Frost, B.R., and Frost, C.D. (2008) A geochemical classification for feldspathic rocks. *Journal of*
660 *Petrology*, 49, 1955–1969.
- 661 Frost, B.R., Swapp, S.M., Frost, C.D., Bagdonas, D.A., and Chamberlain, K.R. (2018)
662 Neoproterozoic tectonic history of the Teton Range: record of accretion against the present-
663 day western margin of the Wyoming Province. *Geosphere*, 14, doi:10.1130/GES01559.1
- 664 Frost, B.R., Frost, C.D., Cornia, M., Chamberlain, K.R., and Kirkwood, R. (2006a) The Teton-
665 Wind River domain: a 2.68-2.67 Ga active margin in the western Wyoming Province.
666 *Canadian Journal of Earth Sciences*, 43, 1489–1510.
- 667 Frost, B.R., Arculus, R.J., Barnes, C.G., Collins, W.J., Ellis, D.J., and Frost, C.D. (2001) A
668 geochemical classification of granitic rocks. *Journal of Petrology*, 42, 2033-2048.
- 669 Frost, C. D., McLaughlin, J.F., Frost, B.R., Fanning, C.M., Swapp, S.M., Kruckenberg, S.C., and
670 Gonzalez, J. (2017) Hadean origins of Paleoproterozoic continental crust in the central
671 Wyoming Province. *Geological Society of America Bulletin*, 129, 259-280.
- 672 Frost, C.D., Swapp, S.M., Frost, B.R., Finley-Blasi, L., and Fitz-Gerald, D.B. (2016)
673 Leucogranites of the Teton Range, Wyoming: a record of Archean collisional orogeny.
674 *Geochimica et Cosmochimica Acta*, 185, 528–549.

- 675 Frost, C.D., Frueh, B.L., Chamberlain, K.R., Frost, B.R. (2006b) Archean crustal growth by
676 lateral accretion of juvenile supracrustal belts in the south-central Wyoming Province.
677 Canadian Journal of Earth Sciences, 43, 1533–1555.
- 678 Frost, C.D., Frost, B.R., Chamberlain, K.R., and Hulsebosch, T.P. (1998) The Late Archean
679 history of the Wyoming Province as recorded by granite plutonism in the Wind River
680 Range, Wyoming. Precambrian Research, 89, 145–173.
- 681 Frueh, B.L. (2002) Archean supracrustal sequences of contrasting origin: the Archean history
682 of the Barlow Gap area, northern Granite Mountains, Wyoming. M.S. thesis, University
683 of Wyoming, Laramie.
- 684 Gao, P., Zheng, Y.-F., and Zhao, Z.-F. (2016) Experimental melts from crustal rocks: a
685 lithochemical constraint on granite petrogenesis. Lithos, 266-267, 133–157.
- 686 Gosselin, D.C., Papike, J.J., Shearer, C.K., Peterman, Z.E., and Laul, J.C. (1990) Geochemistry
687 and origin of Archean granites from the Black Hills, South Dakota. Canadian Journal of
688 Earth Sciences, 27, 57–71.
- 689 Gosselin, D.C., Papike, J.J., Zartman, Z.E., and Laul, J.C. (1988) Archean rocks of the Black
690 Hills, South Dakota: reworked basement from the southern extension of the Trans-
691 Hudson orogen. Geological Society of America Bulletin, 100, 1244–1259.
- 692 Harris, N.B.W., and Inger, S. (1992) Trace element modelling of pelite-derived granites.
693 Contributions to Mineralogy and Petrology, 110, 46–56.
- 694 Holtz, F., and Johannes, W. (1991) Genesis of peraluminous granites I. Experimental
695 investigation of melt compositions at 3 and 5 kb and various H₂O activities. Journal of
696 Petrology, 32, 935–958.

- 697 Johnson, K., Barnes, C.G., and Miller, C.A. (1997) Petrology, geochemistry, and genesis of
698 high-Al tonalite and trondhjemites of the Cornucopia Stock, Blue Mountains,
699 northeastern Oregon. *Journal of Petrology*, 38, 1585–1611.
- 700 Koester, E., Pawley, A.R., Fernandes, L.A.D., Porcher, C.C., Soliani, J.R.E. (2002) Experimental
701 melting of cordierite gneiss and the petrogenesis of syntranscurrent peraluminous granites
702 in southern Brazil. *Journal of Petrology*, 43, 1595-1616.
- 703 Kump, L.R., and Barley, M.E. (2007) Increased subaerial volcanism and the rise of atmospheric
704 oxygen 2.5 billion years ago. *Nature*, 448, 1033–1036.
- 705 Laurent, O., Martin, H., Moyen, J.F., and Doucelance, R. (2014) The diversity and evolution of
706 late-Archean granitoids: evidence for the onset of “modern-style” plate tectonics between
707 3.0 and 2.5 Ga. *Lithos*, 205, 208–235.
- 708 Le Breton, N., and Thompson, A.B. (1988) Fluid-absent (dehydration) melting of biotite in
709 metapelites in the early stages of crustal anatexis. *Contributions to Mineralogy and
710 Petrology*, 99, 226–237.
- 711 Mayne, M.J., Stevens, G., and Moyen, J.F. (2020) A phase equilibrium investigation of selected
712 source controls on the composition of melt batches generated by sequential melting of an
713 average metapelite. In Janousek, V., Bonin B., Collins, W.J., Farina, F., and Bowden, P.,
714 eds, *Post-Archean granitic rocks: petrogenetic processes and tectonic environments*.
715 Special Publication of the Geological Society of London, 491, 223–241.
- 716 McCombs, J.A., Dahl, P.S., and Hamilton, M.A. (2004) U-Pb ages of Neoproterozoic granitoids
717 from the Black Hills, South Dakota, USA: implications for crustal evolution in the
718 Archean Wyoming Province. *Precambrian Research*, 130, 161–184.

- 719 Meredith, M.T. (2005) A Late Archean tectonic boundary exposed at Tin Cup Mountain, Granite
720 Mountains, Wyoming. M.S. thesis, University of Wyoming, Laramie.
- 721 Miller, C.F. (1985) Are strongly peraluminous magmas derived from pelitic sedimentary
722 sources? *Journal of Geology*, 93, 673–689.
- 723 Mueller, P.A., and Wooden, J.L. (2012) Trace element and Lu-Hf systematics in Hadean-
724 Archean detrital zircons: implications for crustal evolution. *Journal of Geology*, 120, 15-
725 29.
- 726 Nabelek, P.I. (2020) Petrogenesis of leucogranites in collisional orogens. In Janousek, V., Bonin
727 B., Collins, W.J., Farina, F., and Bowden, P., eds, *Post-Archean granitic rocks: petrogenetic processes and tectonic environments*. Special Publication of the Geological
728 Society of London, 491, 179–207.
- 730 Nabelek, P.I., and Glascock, M.D. (1995) REE-depleted leucogranites, Black Hills, South Dakota:
731 a consequence of disequilibrium melting of monazite-bearing schists. *Journal of Petrology*,
732 36, 1055–1071.
- 733 Patiño Douce, A.E., Beard, J.S. (1995) Dehydration-melting of biotite gneiss and quartz
734 amphibolite from 3 to 15 kbar. *Journal of Petrology*, 36, 707–738.
- 735 Patiño Douce, A.E., Beard, J.S. (1996) Effects of P, f(O₂) and Mg/Fe ratio on dehydration
736 melting of model metagreywackes. *Journal of Petrology*, 37, 999–1024.
- 737 Patiño Douce A. E., and Harris, N. (1998) Experimental constraints on Himalayan anatexis.
738 *Journal of Petrology*, 39, 689–710.
- 739 Pickering, J., Johnston, A.D. (1998) Fluid-absent melting behavior of a two-mica metapelite:
740 experimental constraints on the origin of Black Hills granite. *Journal of Petrology*, 39,
741 1787–1804.

- 742 Redden, J.A., Peterman, Z.E., Zartman, R.E., and DeWitt, E. (1990) U-Th-Pb geochronology and
743 preliminary interpretation of the tectonic development of Precambrian rocks in the Black
744 Hills. In Lewry, J.F., and Stauffer, M.R., eds., The Early Proterozoic Trans-Hudson
745 Orogen of North Maerica. Geological Association of Canada Special Paper 37, 229-251.
- 746 Shand, S.J. (1947) Eruptive Rocks, 3rd edition. London, Thomas Murray & Co.
- 747 Slagstad, T. (2003) Geochemistry of trondhjemites and mafic rocks in the Bymarka ophiolite
748 fragment, Trondheim, Norway: Petrogenesis and tectonic implications. Norwegian
749 Journal of Geology, 83, 167–185.
- 750 Stoeser, D.B., and Frost, C.D., 2006. Nd, Pb, Sr, and O isotopic characterization of the Saudi
751 Arabian Shield terranes. Chemical Geology, 226, 163–188.
- 752 Stuckless, J.S. (1989) Petrogenesis of two contrasting Late Archean granitoids, Wind River
753 Range, Wyoming. U.S. Geological Survey Professional Paper, 1491, 38p.
- 754 Swapp, S.M., Frost, C.D., Frost, B.R., Fitz-Gerald, D.B. (2018) 2.7 Ga high-pressure granulites
755 of the Teton Range: record of Neoproterozoic continent collision and exhumation.
756 Geosphere, 14, doi:10.1130/GES01607.1.
- 757 Sylvester, P.J. (1998) Post-collisional strongly peraluminous granites. Lithos, 45, 29–44.
- 758 Tang, M., Chen, K., and Rudnick, R.L. (2016) Archean upper crust transition from mafic to
759 felsic marks the onset of plate tectonics. Science, 351, 372–375.
- 760 Taylor, S.R., and McLennan, S.M. (1985) The continental crust: its composition and evolution.
761 Oxford, Blackwell Scientific Publications.
- 762 Van Boening, A.M., and Nabelek, P.I. (2008) Petrogenesis and tectonic implications of
763 Paleoproterozoic mafic rocks in the Black Hills, South Dakota. Precambrian Research,
764 167, 363-376.

- 765 Vielzeuf, D., and Montel, J.M. (1994) Partial melting of metagreywackes Part I. Fluid-absent
766 experiments and phase relations. *Contributions to Mineralogy and Petrology*, 117, 375–
767 393.
- 768 Vincent, S.A. (2017) Neoproterozoic metamorphism and metasomatism during crustal assembly of
769 the southern Wyoming Province. M.S. thesis, University of Wyoming, Laramie.
- 770 Wall, E.N. (2004) Petrologic, geochemical and isotopic constraints on the origin of 2.6 Ga post-
771 tectonic granitoids of the central Wyoming Province. M.S. thesis, University of
772 Wyoming, Laramie.
- 773 Wilks, M.E. (1991) The petrology and petrogenesis of three Late Archean K-rich granites in the
774 Archean Wyoming Province. Ph.D. dissertation, New Mexico Institute of Mining and
775 Technology, Socorro.
- 776 Wood, L.F., and Miller, C.F. (1984) Chemistry and genesis of peraluminous trondhjemite dikes,
777 Blue Ridge, North Carolina-Georgia. *Southeastern Geology*, 25, 13–24.
- 778 Zartman, R.E. and Reed, J.C., Jr. (1998) Zircon geochronology of the Webb Canyon Gneiss and
779 the Mount Owen Quartz Monzonite, Teton Range Wyoming: significance to dating late
780 Archean metamorphism in the Wyoming craton. *The Mountain Geologist*, 35, 71–77.
- 781 Zen, E-an (1986) Aluminum enrichment in silicate melts by fractional crystallization: some
782 mineralogic and petrographic constraints. *Journal of Petrology*, 27, 1095–1117.
- 783 Zhao, G., Sun, M., Wilde, S.A., and Sanzhong, L. (2005) Late Archean to Paleoproterozoic
784 evolution of the North China Craton: key issues revisited. *Precambrian Research*, 136,
785 177–202.
- 786

787
788
789
790
791
792
793
794
795
796
797
798
799
800
801
802
803
804
805
806
807
808
809

Figure captions

Fig. 1. Map of the Wyoming Province, showing locations of Neoproterozoic SPG. Archean rocks of the Wyoming Province are exposed in Wyoming, Montana, and in the Black Hills of South Dakota. The boundary of the Wyoming Province with Proterozoic provinces to the south is exposed only in southeastern Wyoming along the Cheyenne belt (solid line); it is dashed where inferred. The biotite granite of the Bears Ears and Wyoming batholith are grouped together as a single suite of SPG; the others are the Bear Mountain granite, Rocky Ridge garnet granite gneiss, Webb Canyon gneiss, Bitch Creek gneiss, and the Mt. Owen batholith.

Fig 2. (a) Aluminum saturation index (ASI), (b) Modified alkali-lime index (MALI), and (c) Fe-index for Wyoming Neoproterozoic SPG suites. Filled symbols are samples with $ASI > 1.1$, open symbols are samples with $ASI < 1.1$. Circled Wyoming batholith and Bears Ears samples are those from the roof zone of the Wyoming batholith in the northern Laramie Mts. Bear Mt samples marked by yellow squares are granites, yellow squares with plus symbol are trondhjemites. Boundaries for MALI are from Frost et al. (2001) and for Fe-index are from Frost and Frost (2008). Data are compiled on Table OM1 from Bagdonas et al. (2016), Cornia (2003), Da Prat (2020), Frost et al. (2016), Frost et al. (2018), Gosselin et al. (1990), Stuckless (1989), Wall (2004), and Wilks (1991).

Fig 3. Wt.% K_2O content plotted as a function of wt.% Na_2O content for Wyoming SPG. Dashed line indicates $K_2O = Na_2O$. Symbols and data sources as in Fig 2.

810 Fig. 4. CaO/Na₂O v. Al₂O₃/TiO₂ for Wyoming SPG. Symbols and data sources as in Fig 2.

811

812 Fig 5. Zr content (in ppm) vs wt.% SiO₂ for Wyoming SPG, contoured for approximate zircon
813 saturation temperatures (Boehnke et al., 2013). Symbols and data sources as in Fig. 2.

814

815 Fig 6. (a) Rb/Ba v. Rb/Sr and (b) and Sr/Ba v. Rb/Sr for Wyoming SPG. Symbols and data
816 sources as in Fig. 2.

817

818 Fig 7. REE patterns for Wyoming SPG suites. (a) Calcic suites, represented by Webb Canyon
819 and Bitch Creek gneisses, (b) suites entirely composed of SPG, represented by the Rocky Ridge
820 and Bear Mountain granites, and suites composed of both weakly and strongly peraluminous
821 granitic rocks, including the Mount Owen batholith (c), and the Wyoming batholith and Bears
822 Ears granite (d). Data sources as in Fig. 2.

823

824 Fig 8. Experimental results for partial melting of Hb-Pl-bearing rocks (a-c), Ms-Bt-rocks (d-f),
825 and Bt-bearing rocks (g-i). Closed symbols = dehydration melting; open symbols = water excess
826 melting. Data for Hb-Pl-bearing rocks are from Beard and Lofgren (1991). Starting compositions
827 for melt compositions from Ms-Bt-bearing rocks include two-mica gneiss (Castro et al., 1999),
828 muscovite schist (Patiño Douce and Harris, 1998), and metapelite (Pickering and Johnston,
829 1998). Starting compositions for melt compositions from Bt-bearing rocks include biotite gneiss
830 (Holtz and Johannes, 1991; Patiño Douce and Beard, 1995), greywacke (Conrad et al., 1998),
831 synthetic Fe-rich biotite gneiss (Patiño Douce and Beard, 1996), and cordierite-bearing
832 paragneiss (Koester et al., 2002). Data were obtained from the compilation by Gao et al. (2016).

833

834 Fig 9. Experimental and thermodynamically predicted positions of water-excess melting and
835 dehydration melting of Hb-Pl rocks, showing that the water-excess melting reactions that formed
836 the Bitch Creek gneiss took place at lower temperature than the dehydration melting reactions
837 that produced the Webb Canyon gneiss. Modified from Frost et al. (2016).

838

839 Fig 10. CaO/Na₂O and Al₂O₃/TiO₂ ratios of experimental partial melts produced by dehydration
840 and water-excess melting of (a) 2-mica gneiss, schist and metapelitic rocks and (b) graywacke
841 and biotite paragneiss, showing the higher CaO/Na₂O characteristic of the latter. Closed symbols
842 = dehydration melting; open symbols = water excess melting. Sources as for Fig. 8d-f.

843

844 Fig 11. Initial ϵ_{Nd} of Wyoming batholith and Bears Ears granite. Open diamonds represent
845 weakly peraluminous samples and closed diamonds represent strongly peraluminous samples.
846 All samples were intruded at 2.62 Ga; Wyoming batholith and Bears Ears samples are offset
847 slightly for clarity. Also shown are potential magma sources, including the 2.63 Ga Louis Lake
848 Batholith (LLB) in the Wind River Range with which the Bears Ears granite is spatially related,
849 older Archean crust of the Granite and Laramie Mountains, evolved metasedimentary rocks of
850 the Granite Mountains, and juvenile sediments of the southern accreted terranes in the Wind
851 River Range and Granite Mountains. Data from Table OM1, Frost et al. (1998; 2006b; 2017),
852 Fruchey (2002), Meredith (2005), and Wall (2004).

853

854 Fig 12. Initial ϵ_{Nd} of Wyoming batholith and Bears Ears granite as a function of longitude,
855 showing more strongly peraluminous and negative ϵ_{Nd} compositions in the Shirley, Pedro, and

856 Laramie Mountains compared to samples from farther west in the Granite Mountains and Wind

857 River Range. Data from Table OM1.

858

859

860

861

862

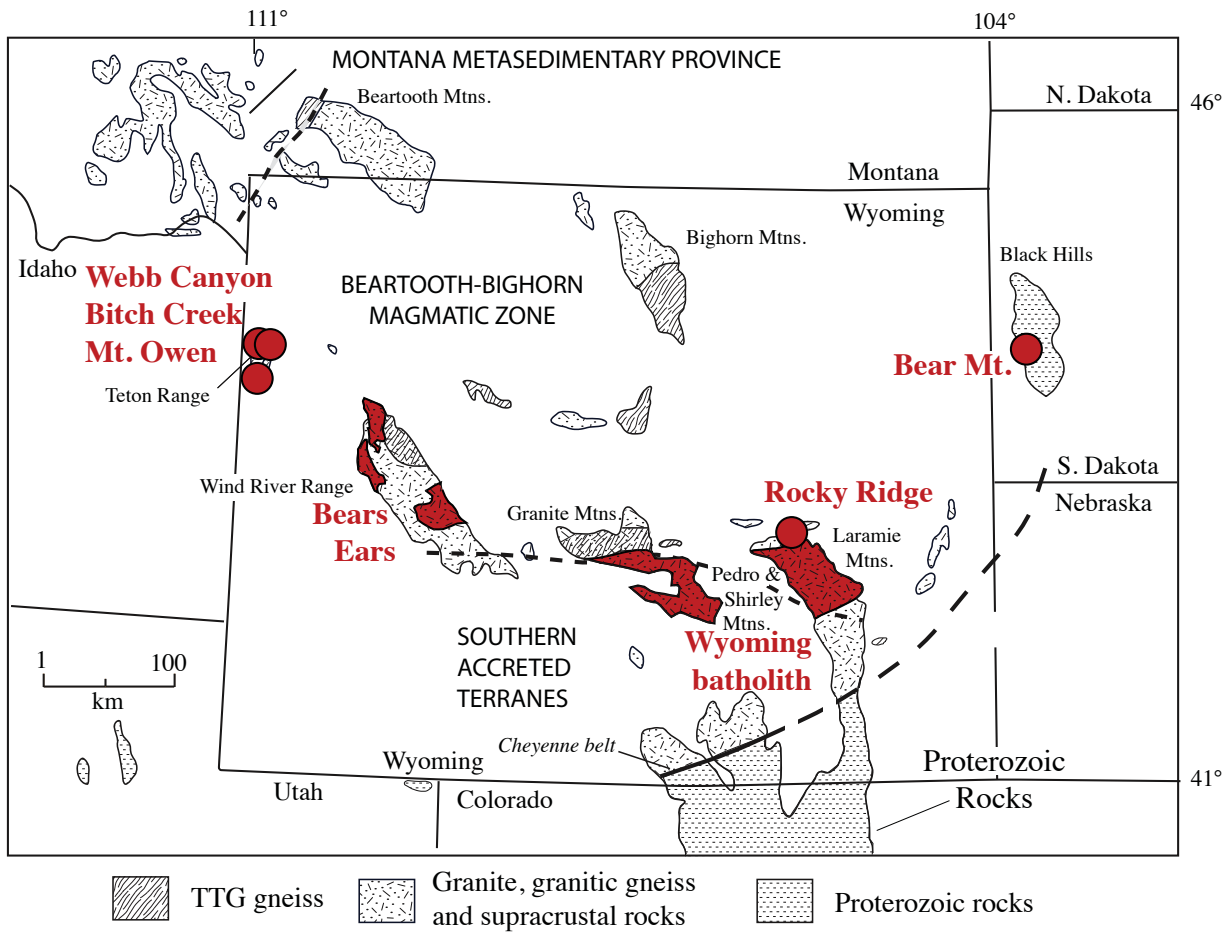


Fig. 1

Fig 2

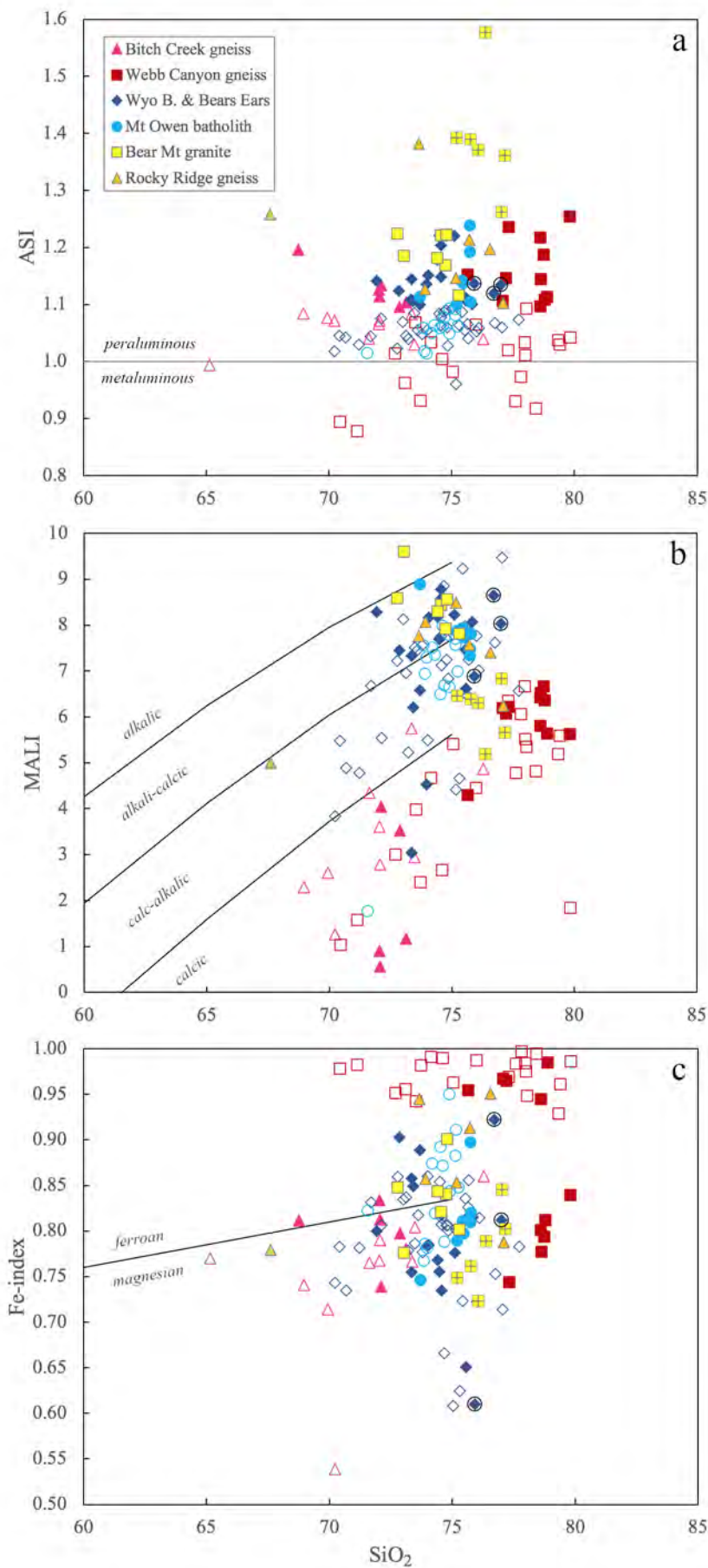


Figure 3

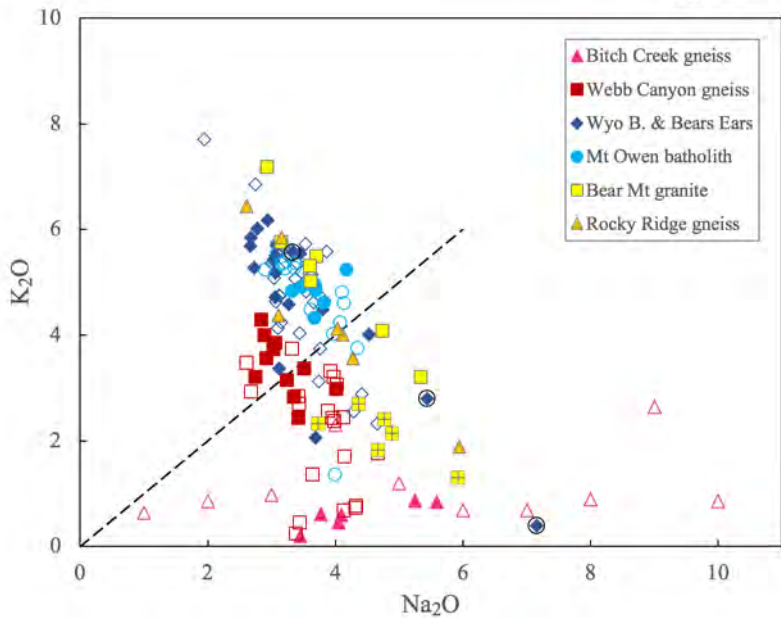


Fig 4

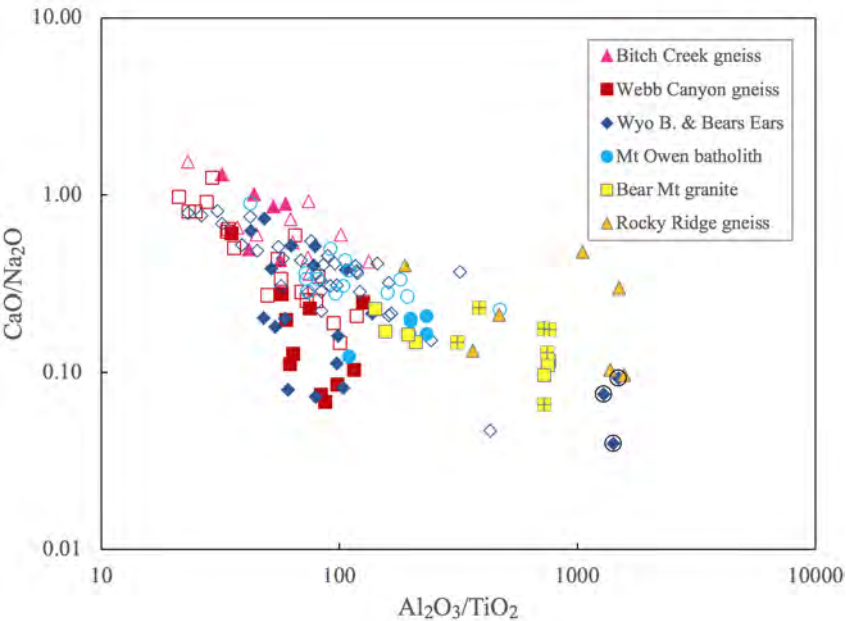


Fig 5

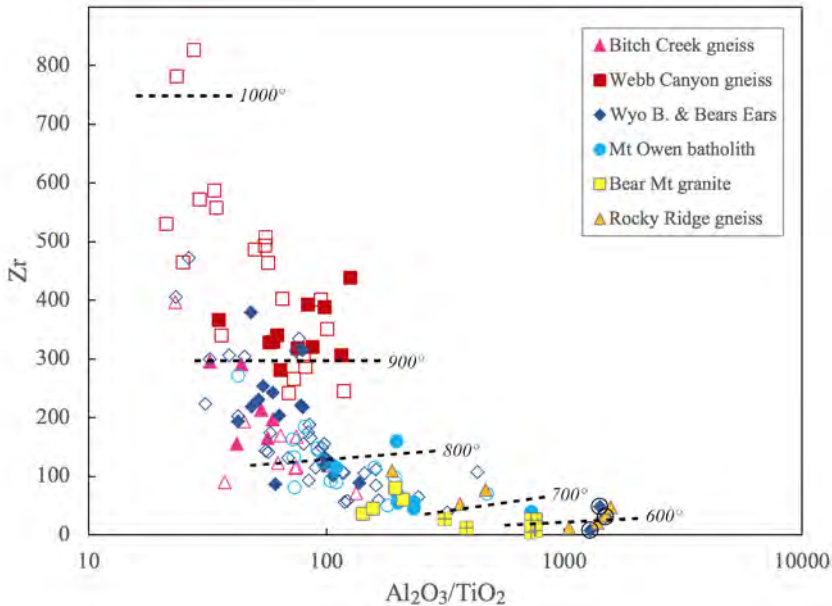
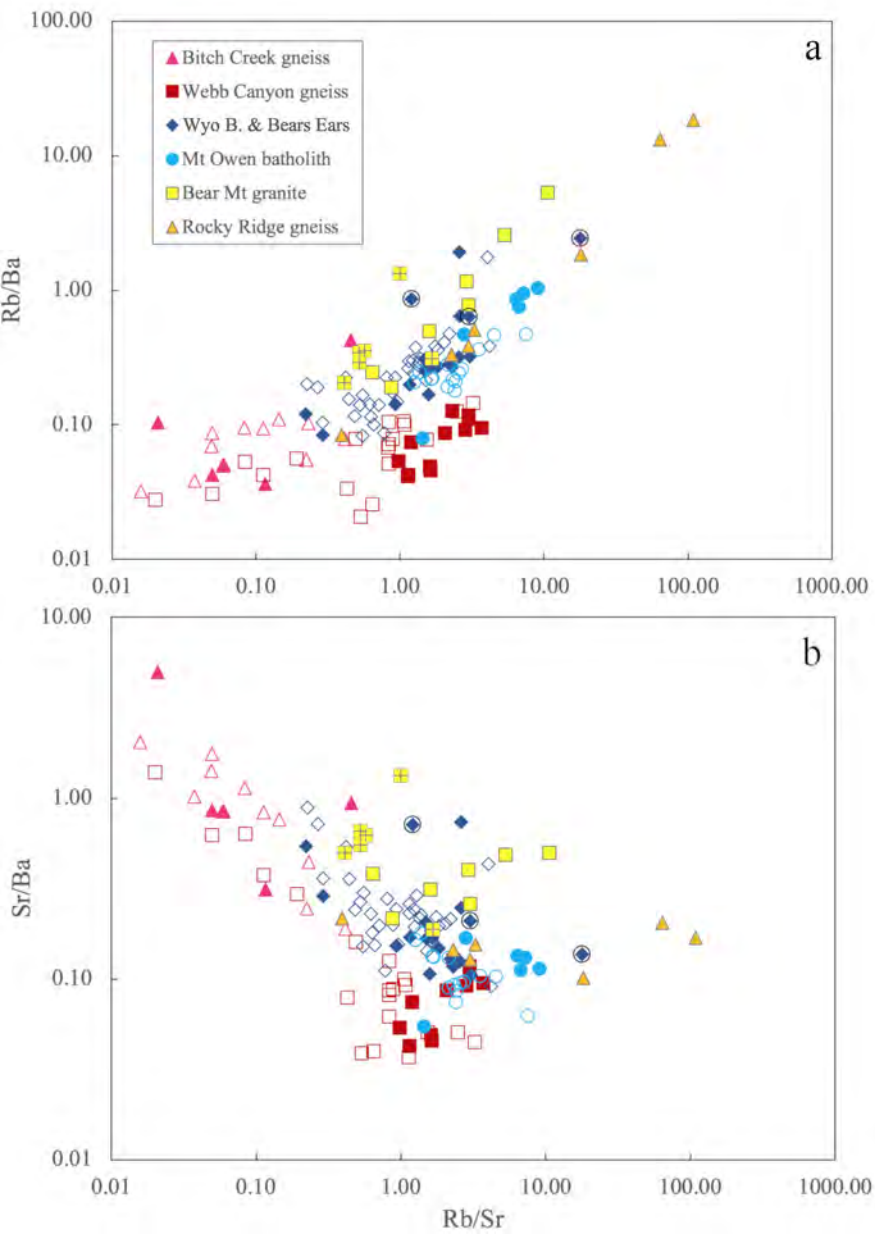
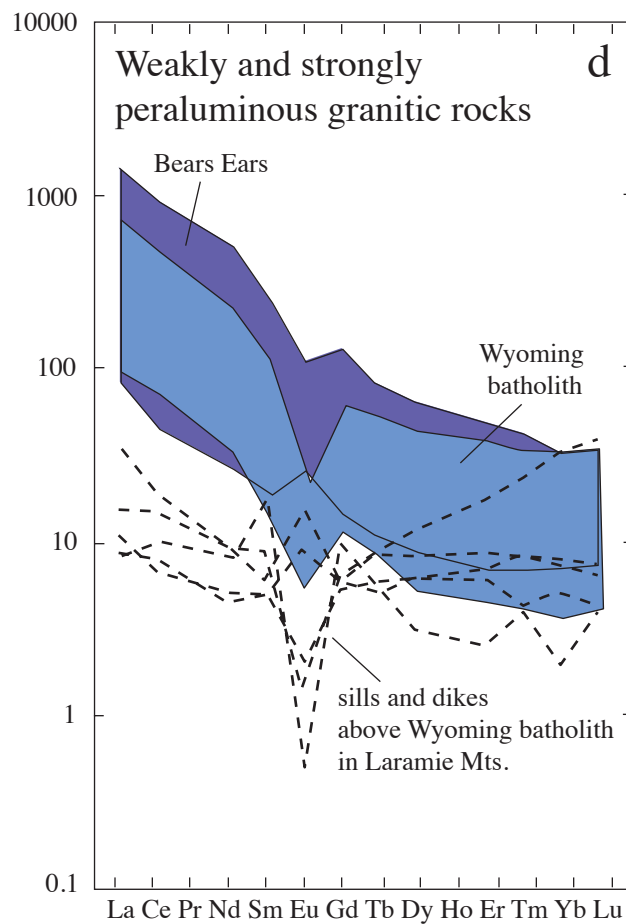
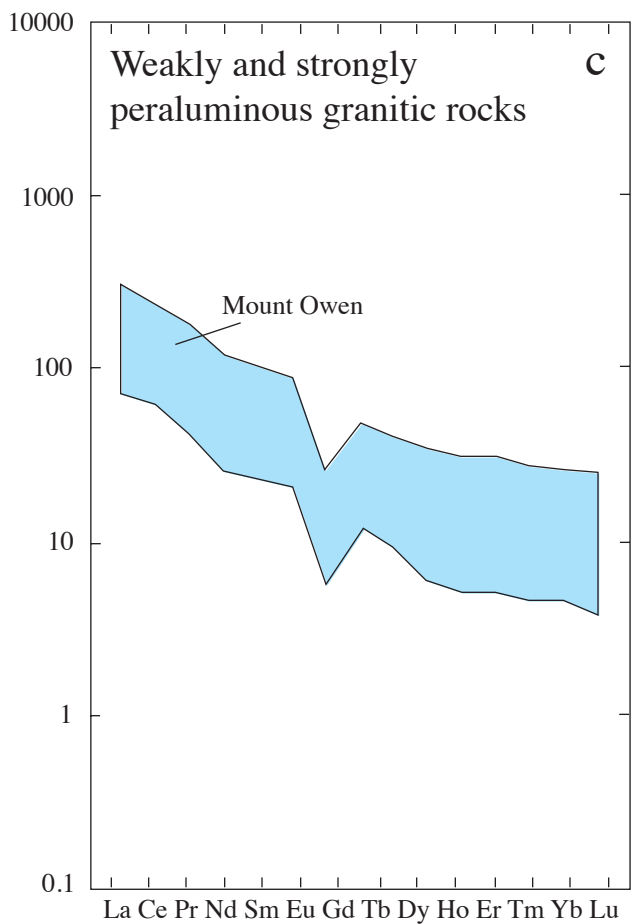
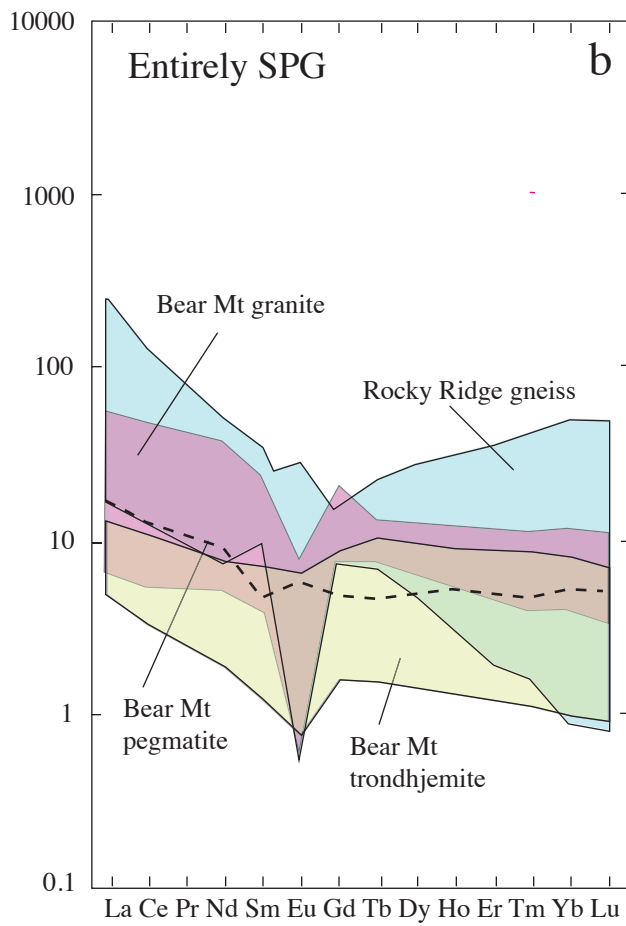
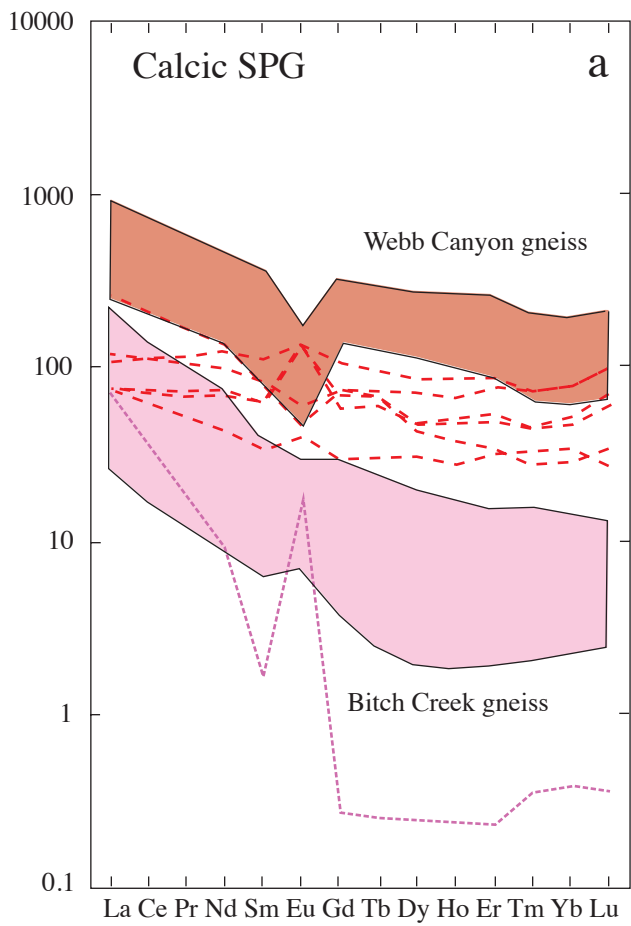
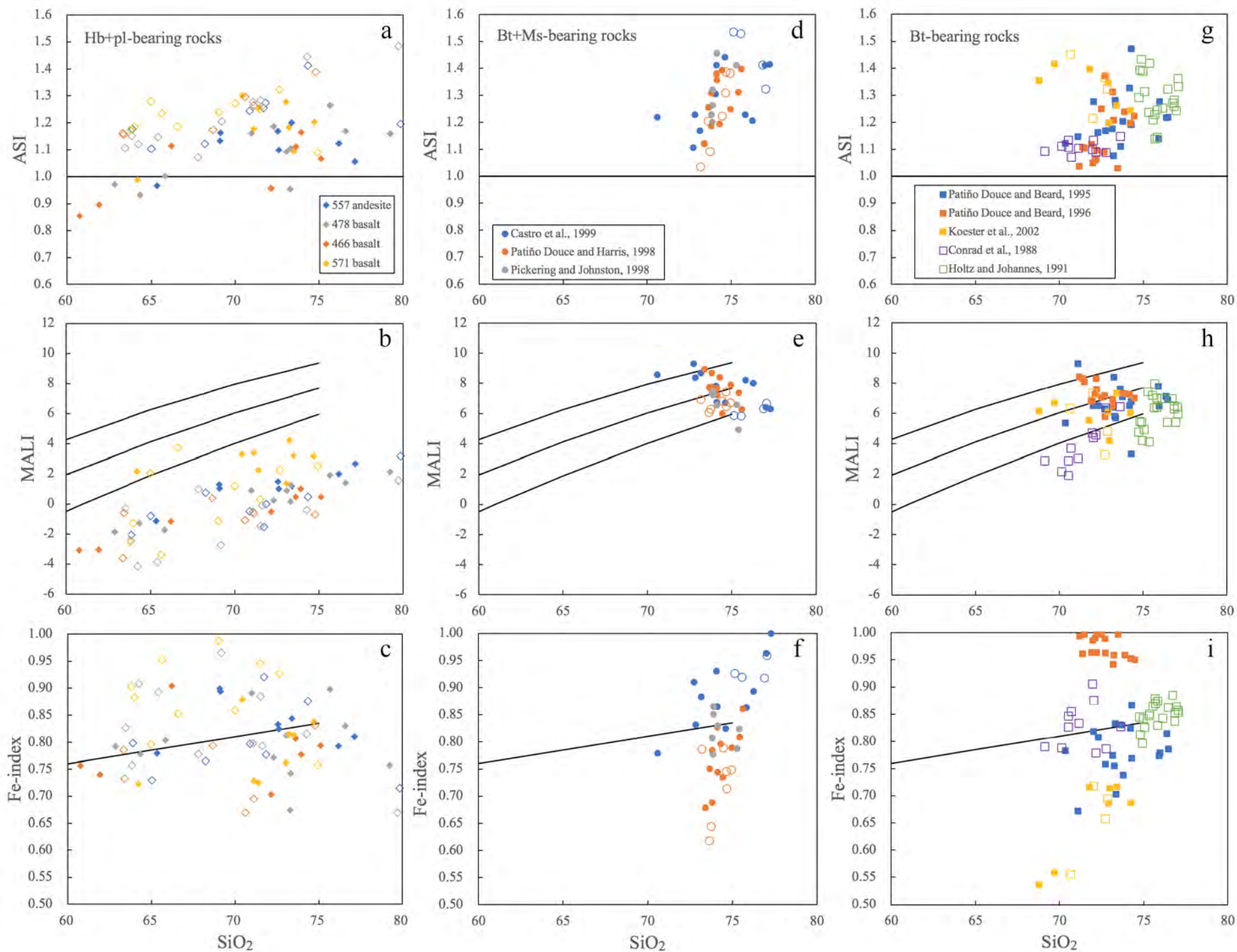


Fig 6







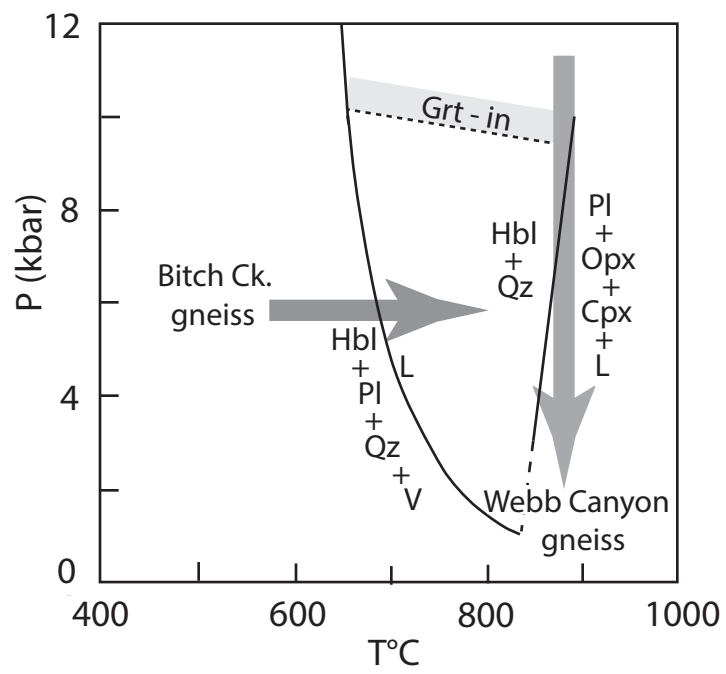


Fig 9

Fig 10

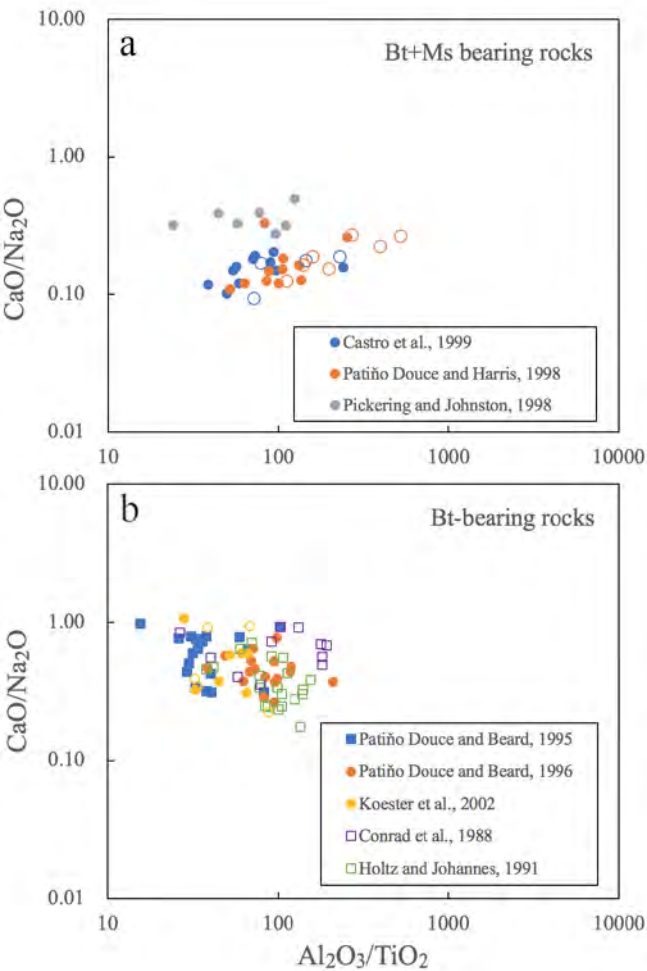


Fig 11.

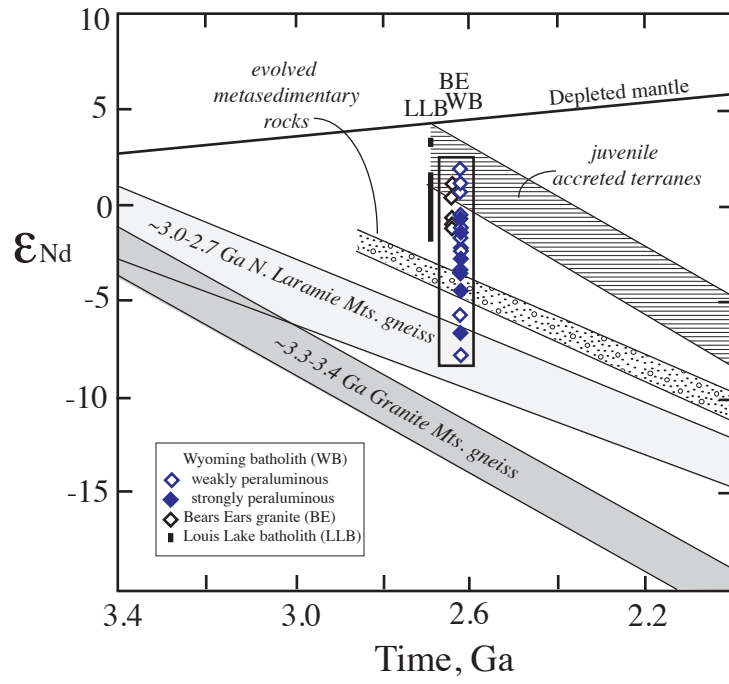


Fig 12

